January 2013

Processing of Advanced Two-Stage CIGS Solar Cells

Manikandan Sampathkumar
University of South Florida, manikandansampath07@gmail.com

Processing of Advanced Two-Stage CIGS Solar Cells

by

Manikandan Sampathkumar

A thesis submitted in partial fulfillment
of the requirements for the degree of
Master of Science in Electrical Engineering
Department of Electrical Engineering
College of Engineering
University of South Florida

Major Professor: Don Morel, Ph.D.
Christos Ferekides, Ph.D.
Andrew Hoff, Ph.D.

Date of Approval:
November 1, 2013

Keywords: Fabrication, Characterization, Large scale manufacture, Throughput, Reproducibility

DEDICATION

This thesis is dedicated to my professor, Dr.Don Morel for his invaluable teachings in my life.

To my parents V.G.Aravinda Nayagi and N.Sampathkumar, who always believed in me and motivated me. To my brother, S.Anirud Kumar, who is a great inspiration in my life.. To my godmother, Kumudha and to my grandparents Gopalan, Patammal Natesan and Picha.

ACKNOWLEDGMENTS

I would like to thank my advisor and one of the best teachers in my life, Dr. Don Morel for providing me an opportunity to work in his lab. His motivation, trust and guidance have made me realize my true potential. I am also greatly indebted to him for the support he provided throughout my Master's program. I would also like to thank Dr. Christos Ferekides for his guidance and suggestions throughout my research. I would like to thank my committee of Dr. Christos Ferekides and Dr. Andrew Hoff for spending their precious time in my defense.

I would like to thank my family for their support and encouragement which has helped me cross several hurdles in my life. A special thanks to my good friend Ryan Anders who taught me everything I know in the lab. I pray for his quick recovery from an accident he encountered and hope that he would make it to the lab soon. I would like extend the special thanks to Kausalya, Seshasayee and Bharath, who always stood beside me in times of trouble. Thanks to my aunty Vasantha who has always helped me in times of need. Thanks to Yejiao Wang, for patiently testing my samples and helping me with my chamber. Thanks to my lab mates Vamsi, Imran, Sara, Shamara, Vasilis and Prasad for making life at the lab livelier. Vamsi and Imran have always shared their experience and thoughts on my research which is greatly appreciated. Thanks to my roommates Anand, Chandramoulee and Anierutan and my friends Riaz, Souki Anusha and Shekar for making life at Tampa more enjoyable. Thanks to Kevin Scott who always helped me with a smiling face. Thanks to Nazuk, who lent me a shoulder in times of distress. I would also like to thank Jay and NREC for providing me an opportunity to work at NREC.

TABLE OF CONTENTS

LIST OF FIGURES iii

LIST OF EQUATIONS vi

ABSTRACT vii

CHAPTER 1: INTRODUCTION 1
1.1 Free Energy 1
1.2 The Idea 2
1.3 Thin Film Solar Cells 2
1.4 CIGS vs Silicon 5
1.5 CIGS and its Properties 6
1.5.1 Ga Graded CIGS Structure 8
1.5.2 Importance of Sodium in CIGS 9

CHAPTER 2: SEMICONDUCTOR AND SOLAR CELL PHYSICS 11
2.1 Semiconductors 12
2.2 P-N Junction 14
2.2.1 Biased P-N Junction 15
2.2.2 Abrupt P-N Junction 16
2.3 Heterojunction 17
2.4 Solar Cells 21
2.4.1 Photocurrent Generation and Spectral Response 22
2.4.2 Current-Voltage (I-V) Characteristics 23
2.4.3 Equivalent Circuit of a Solar Cell 25

CHAPTER 3: DEVICE FABRICATION AND CHARACTERIZATION 28
3.1 Device Structure and Outline 28
3.2 Fabrication Techniques 29
3.2.1 Substrate 29
3.2.2 Molybdenum Back Contact 30
3.2.3 CIGS Thermal Evaporator System 31
3.2.3.1 Fabrication of the CIGS Absorber Layer 34
3.2.4 Chemical Bath Deposition of the N-type Contact 35
3.2.5 ZnO Deposition 36
3.2.6 Front Contact ZnO:Al Deposition 37
3.3 Characterization of the Device 37

3.3.1 Energy Dispersive Spectroscopy (EDS) 37
3.3.2 I-V Characteristics 39

CHAPTER 4: RESULTS AND DISCUSSION 40
4.1 Two-Step Growth Recipe 40
4.2 Controlled Selenium Flux 41
4.3 Growth Recipe Changes 42
4.4 Effect of Growth Recipe Changes 45
4.5 Gradients along the Sample 47
4.6 Improper Sample Storage and Cleaning Process 49
4.7 Nuances in Chemical Bath Deposition 51
4.8 EDS Depth Penetration 53
4.9 I-V Characteristics of the Device 57

CHAPTER 5: CONCLUSIONS AND RECOMMENDATIONS 61

REFERENCES 63

LIST OF FIGURES

Figure 1 Swanson effect 3

Figure 2 Solar cell efficiencies over the years 4

Figure 3 Absorption coefficients of different semiconducting materials 6

Figure 4 Chalcopyrite structure of CIGS 7

Figure 5 Band structure for a) Homogenous CIGS structure b) Graded CIGS structure 9

Figure 6 (a) intrinsic semiconductor (b) p-type semiconductor (c) n-type semiconductor 13

Figure 7 (a) P-N junction (b) Energy band diagram 14

Figure 8 Space charge distribution in an abrupt P-N junction 16

Figure 9 Electric field distribution of an abrupt P-N junction 16

Figure 10 Potential variation of an abrupt P-N junction 17

Figure 11 Energy band diagram of two isolated semiconductors 18

Figure 12 Heterojunction of an ideal P-N heterojunction at thermal equilibrium 18

Figure 13 Band offsets between CGS – CIS – CdS – ZnO 20

Figure 14 I-V characteristics of a solar cell 24

Figure 15 Equivalent circuit of a solar cell a) Ideal solar cell
b) Solar cell with series and parallel resistances 25

Figure 16 Effect of series resistance 26

Figure 17 Effect of shunt resistance 27

Figure 18 Structure of solar cell 28

Figure 19 Thermal evaporator used in CIGS growth 32

Figure 20 Time-Temperature profile for CIGS absorber layer 35

Figure 21 Electron beam - Sample interaction 38

Figure 22 Cu/In and Cu/Ga as a function of Se content 41

Figure 23 Monitored vs Unmonitored Se flux depositions 42

Figure 24 Growth recipe results for process 1 43

Figure 25 Growth recipe results for process 2 44

Figure 26 Metal/III ratios for process 2 44

Figure 27 Copper cut off time 45

Figure 28 Atomic % of elements present in process 1 and process 2 46

Figure 29 % change in atomic percentage of elements between process 1 and process 2 47

Figure 30 Atomic composition of elements for SC-47 48

Figure 31 Thickness variation across the sample 48

Figure 32 Device performance as a result of thickness variation 49

Figure 33 SEM images of molybdenum a) Gradients observed due to polymer storage
b) Contamination observed at 30000X due to polymer storage 50

Figure 34 Imperfections arising due to improper sample cleaning and storage 51

Figure 35 a) Uneven grains due to low spinner speed
b) Even grain growth for an increased spinner speed 52

Figure 36 a) Non uniform deposition due to cluster-by-cluster growth
b) Uniform deposition due to Ion-by-ion growth 52

Figure 37 A depth profile simulation at 25KeV 53

Figure 38 A depth profile simulation at 15KeV 54

Figure 39 EDS analysis on CIGS sample at 25KeV 55

Figure 40 EDS analysis on a CIGS sample at 15KeV 56

Figure 41 Dark I-V for SC-53 57

Figure 42 Light I-V for SC-53 57
Figure 43 Dark I-V for SC-56 58
Figure 44 Light I-V for SC-56 58
Figure 45 Dark I-V for SC-47 59
Figure 46 Light I-V for SC-47 59
Figure 47 Dark I-V for MSC-11 60
Figure 48 Light I-V for MSC-11 60

LIST OF EQUATIONS

Equation 1 Variation of bandgap in CIGS 8

Equation 2 Fermi distribution function 12

Equation 3 Built in potential 15

Equation 4 Width of the depletion region 15

Equation 5 Discontinuity in the conduction band 19

Equation 6 Discontinuity in the valence band 19

Equation 7 Photon energy greater than bandgap for conduction 21

Equation 8 Absorption of light 21

Equation 9 Generation rate of photo carriers 22

Equation 10 Spectral response 22

Equation 11 Photocurrent density 23

Equation 12 Dark current of a solar cell 23

Equation 13 Photocurrent under illumination 23

Equation 14 Open circuit voltage 23

Equation 15 Photo generated current 24

Equation 16 Fill factor 25

Equation 17 Efficiency of a solar cell 25

ABSTRACT

An advancement of the two stage growth recipe for the fabrication of CIGS solar cells was developed. The developed advancement was inconsistent in producing samples of similar stoichiometry. This was a huge barrier for up scaling the process as the behavior of devices would be different due to variation in stoichiometry. Samples with reproducible stoichiometry were obtained once the heating rate of elements, selenium in particular was better understood. This is mainly attributed to the exponential increase of selenium flux after its evaporation temperature. Monitoring the selenium flux was vital in getting constant selenium fluxes. Few changes to the growth recipe were induced to optimize the amount of selenium being used. Depositions were done using constant selenium to metal flux ratio of 5. Elemental tradeoffs were observed as a result of the growth recipe change. These tradeoffs are in favor of the two stage growth recipe. The solar cells were fabricated on a soda lime glass substrate with a molybdenum back contact. Improper sample cleaning and storage were found to affect the deposition outcome of the molybdenum back contact. This also had a cascading effect on the absorber layer. Residual precipitates during deposition of CdS were avoided by increasing the spinner speed which increased the reaction rate. This is attributed to the growth of CdS either by cluster-by-cluster growth or by ion-by-ion growth. SEM, EDS were some important tools used to characterize the devices. EDS in particular, was used extensively at different stages throughout the growth process to ensure that we were heading in the right direction. Current-voltage (I-V) measurements were done to study the solar cell performance under light and dark.

CHAPTER 1: INTRODUCTION

"I have no doubt that we will be successful in harnessing the sun's energy. If sunbeams were weapons of war, we would have had solar energy centuries ago." - Sir George Porter, Nobel Laureate in Chemistry.

1.1 **Free Energy**

The growing demand for energy and a limitation on its major source (fossil fuels) has proved to be a huge concern for the human race. The initial availability of fossil fuels was taken for granted and the importance of renewable energy was not realized until the mid-1970. The oil embargo by the Arab countries during this period had a huge price inflation on the crude oil barrels .This emphasized the necessity for dependent sources of energy. Renewable energy sources are dependent sources of energy because they are continuously replenished. The sun is an energy source with a 10billion year lifetime. This easy availability and accessibility makes solar energy a stand out in the renewable energy department.

The creation of electric current in a material upon light exposure is called photovoltaic effect. Solar cells are semiconductor materials which exhibit photovoltaic behavior. Although solar cells for terrestrial applications were used as early as 1958, their commercial growth is slow. Solar cells should satisfy an optimum cost to efficiency ratio for commercial success. Thin film technology has the capability to give a low cost to efficiency ratio. Solar cells manufactured using this technology have thin layers of photovoltaic materials to give high efficiency. Permutation in the order of deposition can further reduce the cost of thin film solar cells. This study involves CIGS thin film solar cells manufactured in a certain order which makes it commercially viable.

1.2 The Idea

The generation of electric current in a material upon light exposure was first observed by Edmund Bequerel in 1839 [1]. The explanation of this effect can be derived from the photoelectric effect. Photoelectric effect describes light as packets of energy called photons. When photons are incident on a material's surface, they transfer their energy to the electrons in the material. If a photon has energy greater than the work function or binding energy of an electron, the electron is released. Photoelectric effect and photovoltaic effect are similar except for the fact that in photoelectric effect the incident light excites the electron all the way to the vacuum level whereas in photovoltaic effect the incident light excites the electron to a new energy level where it is free to move within the material. When photovoltaic effect takes place in a material which has a built-in electric field, the electrons can be made to flow in a certain direction. This constant flow of electrons is the electric current, and by placing conductive metal contacts, we can tap this current out for external use. The tapped current multiplied with the voltage (the built-in electric field) defines the power that a solar cell can produce.

1.3 Thin Film Solar Cells

In 1954, solar cells were first commercially manufactured at Hoffman Electronics Corporation. They started making use of solar cells for toys and other minor uses [2]. The costs of their solar cells were $250 per watt and this was almost hundred times more than the cost per watt produced by coal at that time. At present we are able to manufacture solar cells for as low as $0.7 per watt. A decline rate for the cost of crystalline silicon solar cells is forecasted by Richard Swanson, the founder of SunPower Corporation. Swanson's law states that, the cost of the photovoltaic cells needed to generate solar power falls by 20% with each doubling of global manufacturing capacity [3].

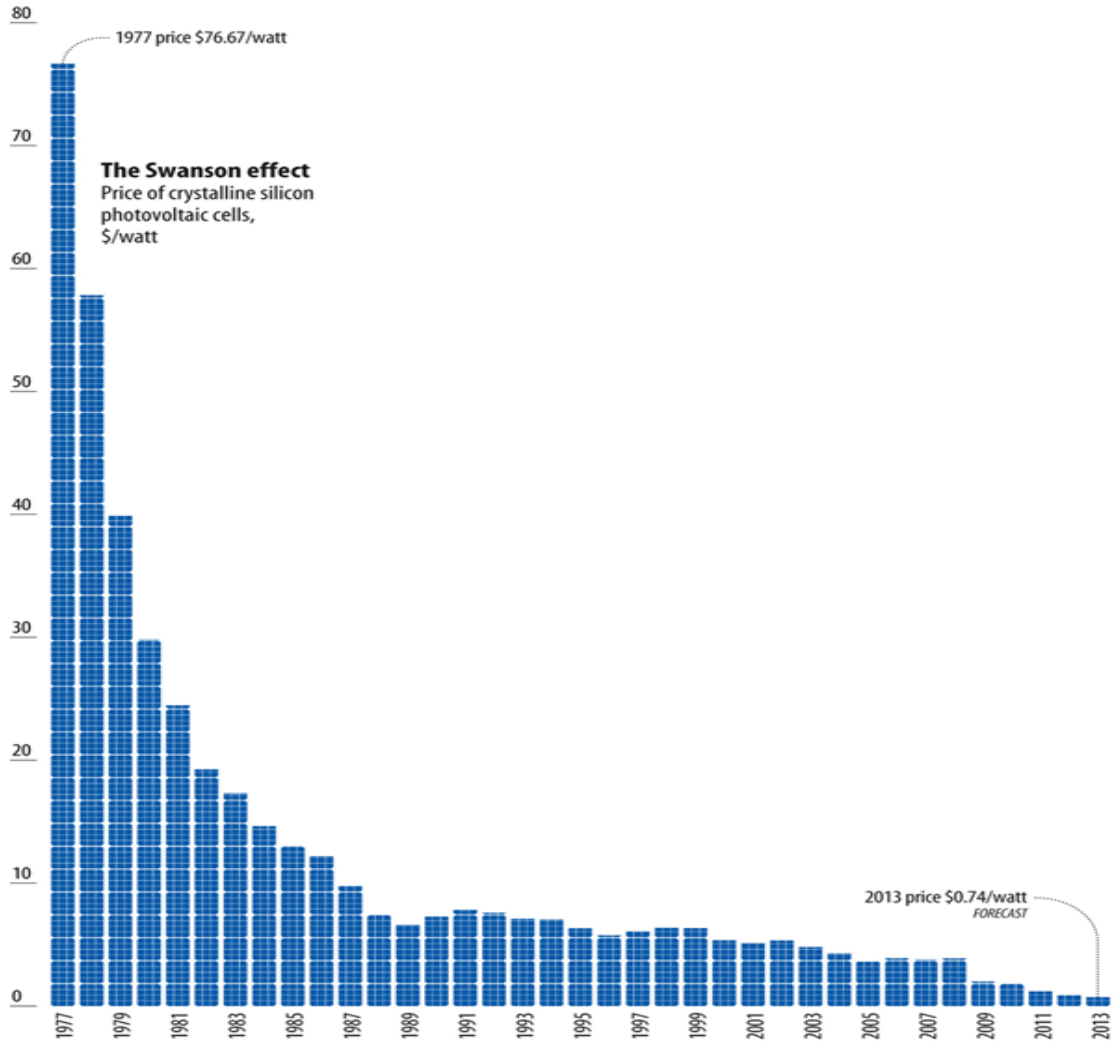

Figure 1 Swanson effect [4]

Along with cost/watt, another important parameter is the efficiency. Having a low cost/watt and low efficiency is going to make the solar module less worthy. Thin film technology has the edge of making high efficiency devices using lower cost. Since only a thin coating of the light absorbing material is used, they promise a lower cost in their making .They also have the flexibility in forming semiconductor films of various compositions through vacuum deposition techniques such as physical vapor deposition , chemical vapor deposition and sputtering .Some of the non-vacuum thin film fabrication techniques such as spray pyrolysis and solution growth

doesn't require expensive equipment for manufacture and can be carried out with cheap labor due to the simplicity of the process. The manufacture of thin film materials on flexible substrates can further reduce the cost as they can be easily transported and manufactured on a large scale.

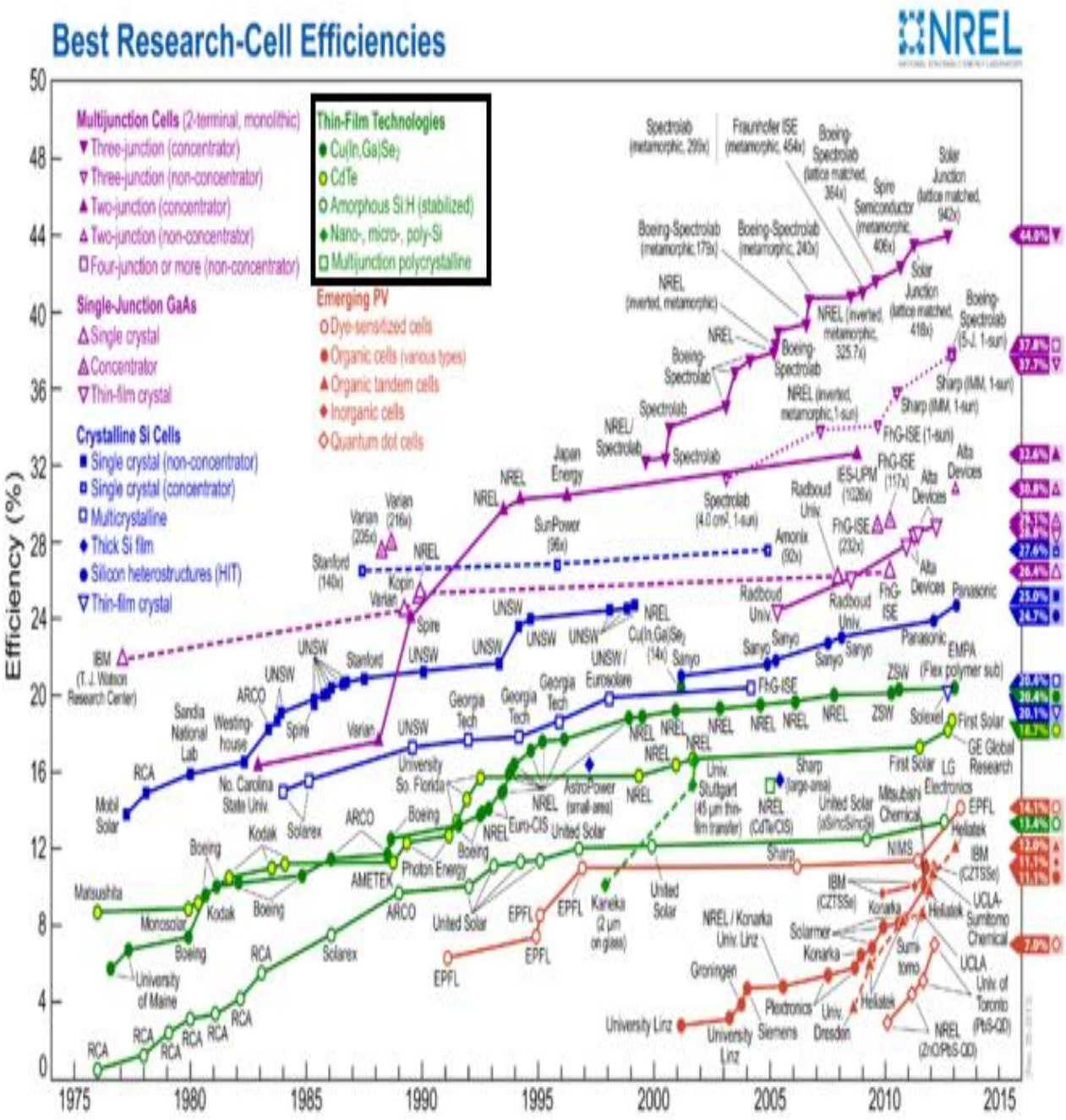

Figure 2 Solar cell efficiencies over the years [5, Public Domain Image]

Figure 2 gives an overview of the best solar cell efficiencies so far .Even though the efficiencies of multijunction cells, single junction GaAs and crystalline Si cells are more than thin film technology; they involve an increased cost in their making. CIGS can be manufactured for a lesser cost per watt for the same range of efficiencies as multijunction cells, single junction GaAs, crystalline Si cells and other thin film technologies.

1.4 CIGS vs Silicon

Swanson's effect shows that the cost/watt of crystalline solar cells to be dropping rapidly, so what is the need for an alternative material?

1. The absorption coefficient of CIGS is 3 x 10^5 cm^{-1}, it requires only a thin layer of CIGS (~1µm) to collect 99% of sunlight. Si is an indirect bandgap material and requires more amount of material (~100-200) µm to collect the same amount of sunlight as CIGS. There is an effective use of raw material in CIGS.

2. CIGS can be manufactured on flexible substrates unlike Si. Flexible substrates allow CIGS to be manufactured using a roll-to-roll process. Roll-to-roll process allows CIGS to be continuously processed rather than in batches and this significantly reduces the processing cost. The easy transportation of the flexible solar modules reduces the transportation cost too.

3. The energy payback time (the time taken for the cell to generate enough energy to offset the energy used for its manufacturing) is comparatively low for CIGS when compared to Si.

Figure 3 shows the absorption coefficient vs incident photon energy of various semiconducting materials used for solar cell development. From the figure we can see that $CuInSe_2$ (Copper Indium Selenide or CIS) clearly has a wider absorption spectrum when compared to other materials. CIGS has an absorption spectrum very similar to CIS.

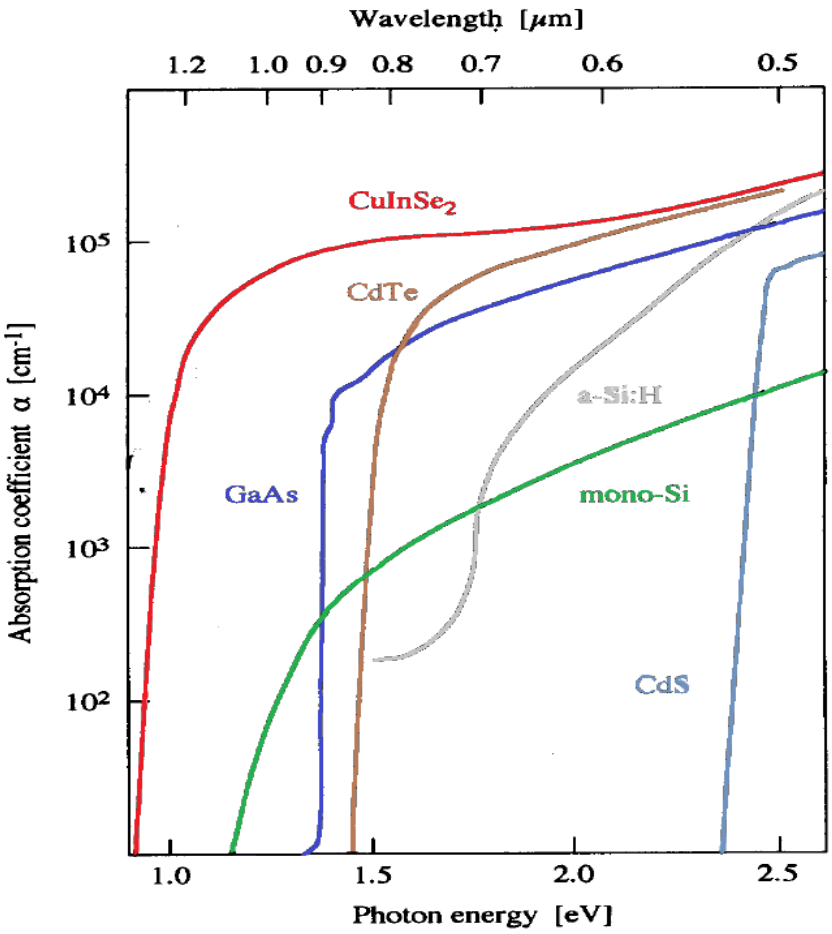

Figure 3 Absorption coefficients of different semiconducting materials [6]

1.5 CIGS and its Properties

CIGS is a I-III-VI quaternary compound belonging to the chalcopyrite family. The chemical formula for CIGS is $CuIn_xGa_{(1-x)}Se_2$, the value of x varies from 0 to 1. If the value of x is 0, the compound becomes copper gallium selenide and if it is 1, the compound becomes copper indium selenide. CIGS is used as an absorbing layer of a solar cell. It is usually deposited on a molybdenum back contact. The order of deposition for a solar cell is as follows: Glass substrate / molybdenum / CIGS / CdS / ZnO / ZnO:Al. The chalcopyrite structure of CIGS is shown in figure 4.

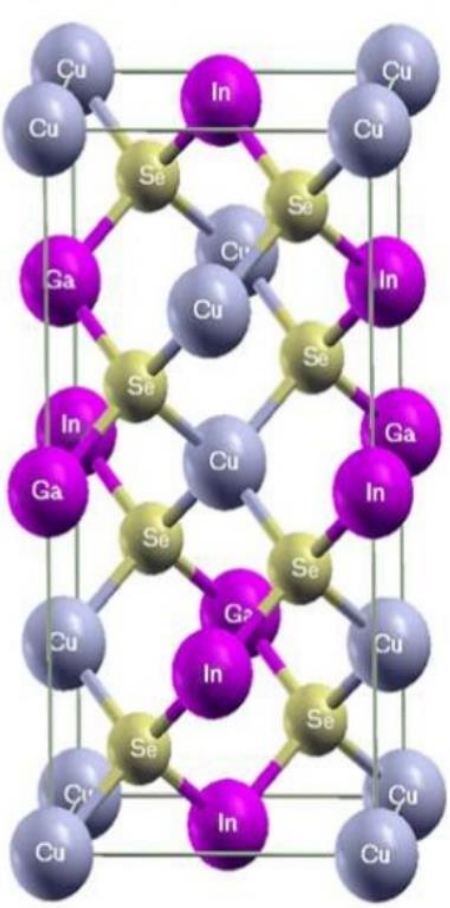

Figure 4 Chalcopyrite structure of CIGS [7]

The absence of atoms from their respective places leads to defects. CIGS is self doping semiconductor and its type is decided by defects (antisite defect, vacancy defect and interstitial defect).The acceptor type (p-type) defects include copper vacancies and copper on indium antisite and the donor type (n-type) defects include indium on copper antisite and selenium vacancies. If the CIGS film is copper rich, it tends to be more p-type due to copper on indium antisite defect. If the CIGS film is In rich, the film can be n-type or p-type due to the existence of indium on copper antisite and copper vacancies at the same time. This is called compensation effect. The copper rich CIGS film has a bad (usually shorted) junction due to the presence of highly conductive copper selenide.

1.5.1 Ga Graded CIGS Structure

The bandgap of pure $CuInSe_2$ is 1.0ev and that of pure $CuGaSe_2$ is 1.7ev, the compounds can be alloyed to get intermediate bandgaps [8]. One of the main advantages of CIGS is the flexibility in varying the material properties as a function of film depth. The required material properties can be achieved by alloying the elements at different rates. Graded structures improve the cell's performance in many ways. The absence of graded bandgaps in solar cells means that there is no drift force outside the depletion region .This absence will force the carriers to rely solely on diffusion, and if the carriers are generated much further than a diffusion length away from the edge of the depletion region, they have a low probability of being collected through the contacts [9].Devices without a graded structure, start to lose current and fill factor while gaining little voltage if the bandgap is increased beyond 1.25ev [9].The value of electron affinity varies with the Ga concentration and this idea is used in devices to have a graded bandgap. Thus by controlling the Ga concentration, a graded bandgap can be engineered. The most successful 3 stage process results from a certain depth profiling of the Ga/(Ga+In) ratio which is believed to contribute to the excellent performance of the cells [8].The variation of bandgap in $CuIn_{(1-x)}Ga_xSe_2$ is given by Eq 1 [10] :

$$E_g = 1.011 + 0.664x - 0.249x\,(1-x)$$

Equation 1 Variation of bandgap in CIGS

The variation of the bandgap according to the above equation is nonlinear and it is referred to as optical bowing. The grading of Ga also provides the absorber layer with a good adhesion to the back contact. Gabor reports the formation of a back surface field near the back contact due to the strong tendency of Ga to move towards the back of the device. This back surface field is similar

to an electric field, it reflects the minority carriers back to the p-n junction and prevents them from recombining with the back contact [9].The shifts in conduction band with and without Ga grading can be seen in the figure below.

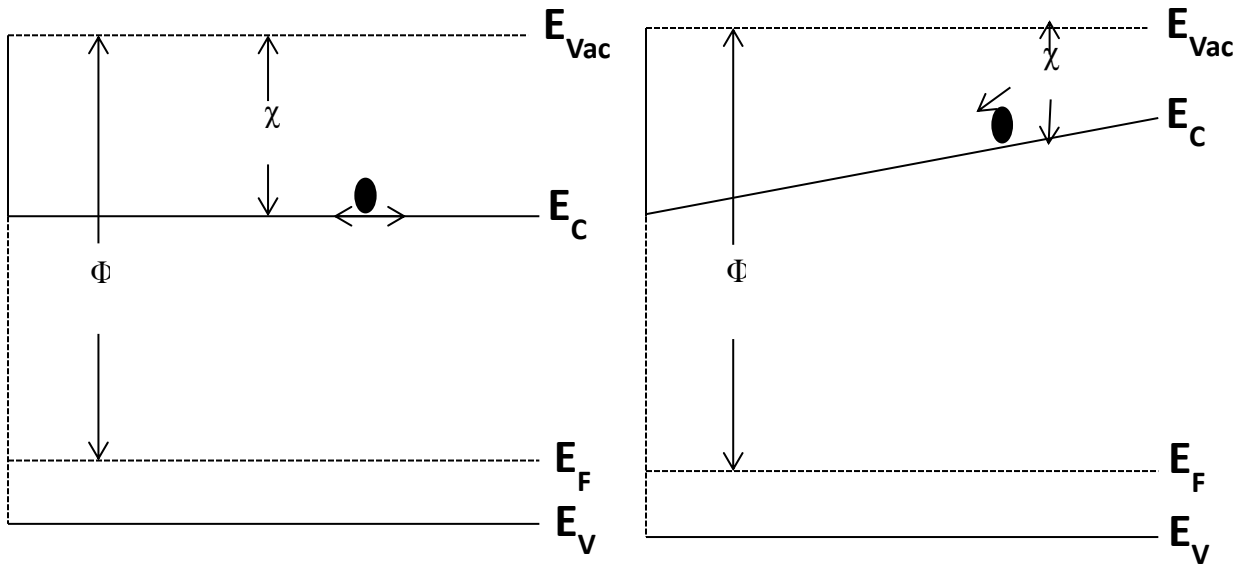

(a) **(b)**

Figure 5 Band structure for a) Homogenous CIGS structure b) Graded CIGS structure

1.5.2 Importance of Sodium in CIGS

The importance of sodium's incorporation was initiated by Hedström and his workers in 1993. Although our process involves sodium diffusion from SLG, the absence of sodium in flexible substrates makes it a necessity quantity to be provided externally. The sodium from SLG diffuses into molybdenum from glass and into CIGS absorber layers from molybdenum. Some of the effects of sodium in CIGS are:

1. Sodium's diffusivity increases the overall conversion efficiency. Its effect is mainly seen by the increase of open circuit voltage (V_{oc}) and fill factor (FF), although there is not much effect on the short circuit current [11].

2. The performance of the cells is found to be more homogenous; however care should be taken as too much diffusivity can cause the device to degrade [11].
3. An increase in sodium diffusivity is found to increase the carrier concentration [12].
4. Although changes in material properties such as increase in mobility and homojunction formation have been linked to the diffusivity of sodium, their influence on the efficiency of the device is minimal. The most influential effect due to sodium diffusivity in the efficiency is linked to the passivation of grain boundary defects by sodium [12].

CHAPTER 2: SEMICONDUCTOR AND SOLAR CELL PHYSICS

The physics of a solar cell has its roots in semiconductors. Understanding the physics of semiconductor is essential in order to understand the operation and working of solar cells.

The nature of a material is described by the band theory of solids. The band theory of solids is a concept derived from the energy levels of an atom. The atom consists of nucleus and electrons. A material consists of zillions of atoms placed periodically with a certain distance from each other. This distance is called as the inter-atomic distance. The atoms are placed close enough for the orbitals of each atom to overlap with one another leading to a series of bands called "energy bands". These energy bands explain the nature and behavior of materials.

The highest range of electron energy level where an electron is present at zero temperature is termed as the valence band. Valence band can be related to the outer most electrons that bonds successive atoms. They can be broken and used for conduction. The unoccupied energy bands which can accommodate electrons energies strong enough to break the binding energy of an atom are termed as conduction bands. Conduction bands can be visualized as the atomic lattice which allows the free movement of delocalized electrons.

Metals, insulators and semiconductors can be easily classified according to the band theory. In a metal, the valence band and conduction band are overlapped. It symbolizes that the electrons are free to move within the lattice of the material and hence has a high conductivity. In an insulator, the valence band and conduction band are separated by a large energy gap and so a lot external energy is required for the electrons to make it to the conduction band. Thus conduction is not

easily possible in an insulator. Semiconductors are materials whose conductivity lies between a metal and an insulator. Semiconductors have their energy bands separated but with a permissible gap. The electrons can make it to the conduction band with a certain amount of external energy.

2.1 Semiconductors

Semiconductors are classified as intrinsic or extrinsic semiconductors based on their impurity level. An intrinsic semiconductor is extremely pure and devoid of any impurities whereas an extrinsic semiconductor has externally added impurities to it. The process of externally adding impurities to a semiconductor (say Si) is termed doping. The extrinsic semiconductor is a n-type semiconductor if the added impurity is a donor impurity (an atom having 5 valence electrons in the outermost shell) and it is a p-type semiconductor if the added impurity is an acceptor impurity (an atom having 3 valence electrons in the outermost shell).Pauli's exclusion principle states that "fermions cannot exist in identical energy states". Considering the fact that electrons are fermions, they obey Pauli's exclusion principle .At zero temperature the electrons start arranging themselves from the lowest available energy state to form a heap of electrons. The fermi energy is defined as the surface of the heap of electrons at absolute zero. The electrons will not have enough energy to rise up above this surface at absolute zero. For any temperature above 0K, electrons are continuously excited to different energy levels and we can only give the probability of where the electron can sit. The fermi level is defined as the energy level with 50% probability of occupation. The fermi distribution function is given by:

$$F(E) = \frac{1}{1 + e^{(E-E_F)/kT}}$$

Equation 2 Fermi distribution function

The band diagram uses fermi level as the base for describing a p-type, n-type or intrinsic semiconductor. The semiconductor can be identified by the position of the fermi level.

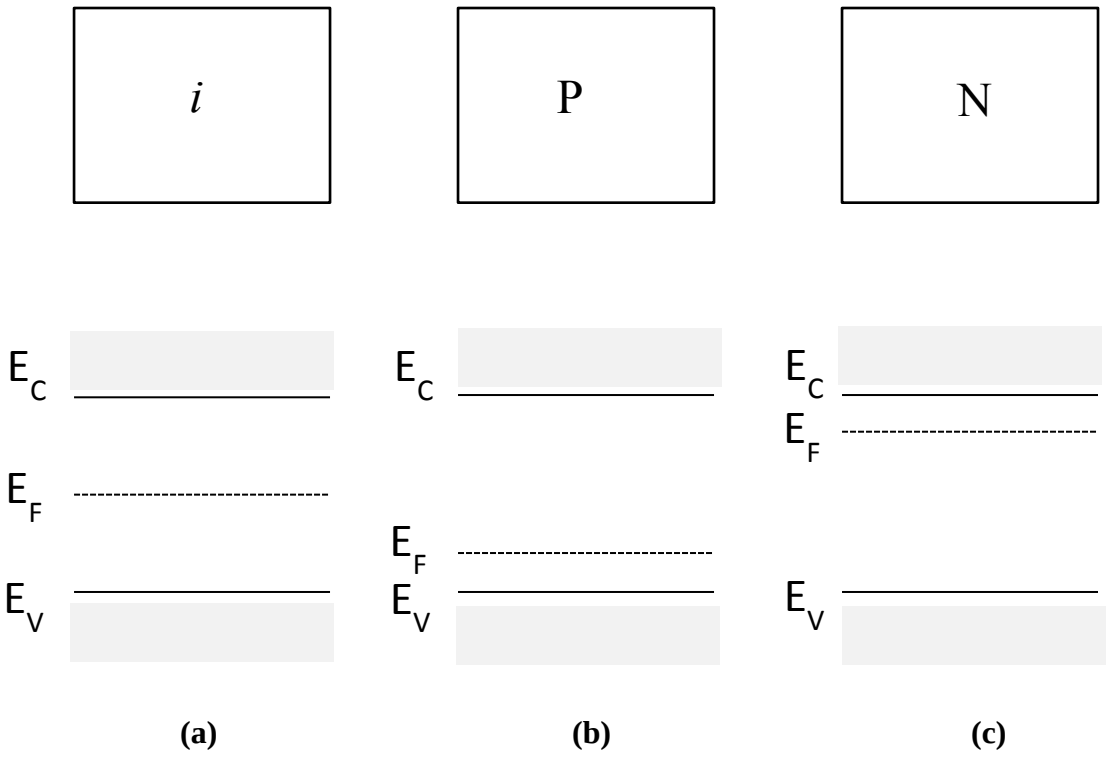

Figure 6 (a) intrinsic semiconductor (b) p-type semiconductor (c) n-type semiconductor

In the above figure, E_C represents conduction band energy, E_V represents valence band energy and E_F represents fermi energy. In figure 6(a), the Fermi level is exactly at the center, meaning no external impurities were added. This says that the material is an intrinsic semiconductor and it is denoted by *i* in the figure. In figure 6(b), the Fermi level is more towards the valence band energy and this tells us that the semiconductor is doped with an acceptor impurity and there are more holes than electrons (p-type). The p-type semiconductor is denoted by P in the figure. Figure 6(c) has its Fermi level more towards the conduction band energy, meaning the semiconductor was doped with a donor impurity and it has more electrons than holes (n-type). The n-type semiconductor is denoted by N in the figure.

2.2 P-N Junction

When a p-type semiconductor and a n-type semiconductor are brought in contact with each other, a P-N junction is formed. During P-N junction formation, the holes flow from the p-type semiconductor to the n-type region leaving behind ionized acceptors and the electrons flow from the n-type semiconductor to the p-type semiconductor leaving behind ionized donors. When this happens, the fermi energy of both the p-type and n-type semiconductors reaches equilibrium. The region which consists of the ionized donors and acceptors are called depletion region as they are depleted of charge carriers. They can also be called as space charge region. The presence of charges of opposite polarity in the space charge region gives rise to a potential difference across the junction. This built in electric field in a P-N junction is called as built-in potential (V_{bi}).

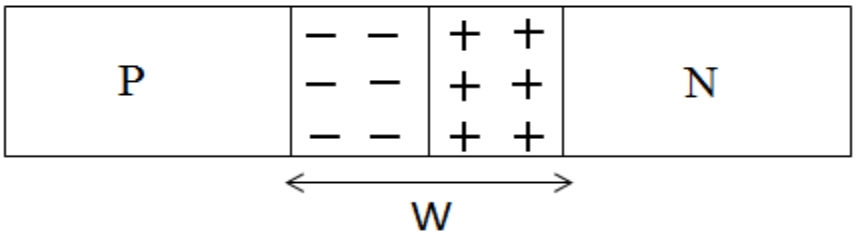

(a)

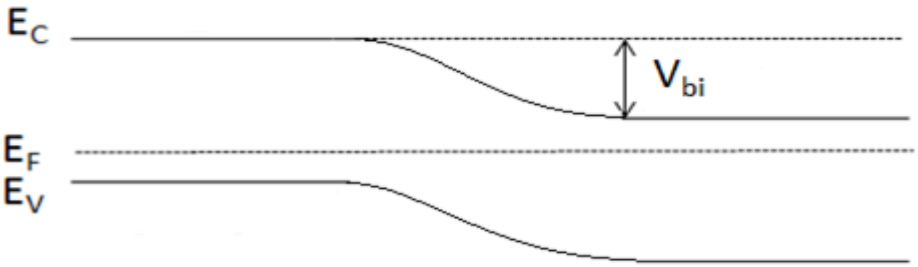

(b)

Figure 7 (a) P-N junction (b) Energy band diagram

The built in potential is given by:

$$V_{bi} = (kT/q) * \ln(N_A N_D/n_i^2)$$

Equation 3 Built in potential

The width of the depletion region is given by:

$$W = [2\varepsilon * (N_A+N_D) V_{bi}]^{1/2} / [q * (N_A N_D)]^{1/2}$$

Equation 4 Width of the depletion region

V_{bi} and W represent the built in potential and the width of the depletion region. N_A represents the acceptor impurity concentration on the p-side of the junction whereas N_D represents the donor impurity concentration on the n-side of the junction. T is the temperature, q is the charge of an electron, k is the Boltzmann constant, n_i is the intrinsic carrier concentration and ε is the dielectric constant.

2.2.1 Biased P-N Junction

When external power supply is given to a P-N junction it is said to be biased. When the positive terminal of the power supply is connected to the p side and the negative terminal of the power supply is connected to the n side of the junction, the P-N junction is forward biased. During forward bias there is a reduced potential energy barrier. The majority carriers from p and n side of the junction tend to crossover this reduced potential energy barrier resulting in diffusion current. When the positive terminal of the power supply is connected to the n side and the negative terminal of the power supply is connected to the p side of the junction, the P-N junction is reverse biased. During reverse bias, the majority carriers are attracted to the power supply and hence there is no diffusion current.

2.2.2 Abrupt P-N Junction

When the impurity concentration in a P-N junction abruptly changes from acceptor impurities (N_A) to donor impurities (N_D) and vice versa, an abrupt P-N junction is formed. If $N_A >> N_D$ or vice versa, a one sided abrupt junction is formed.

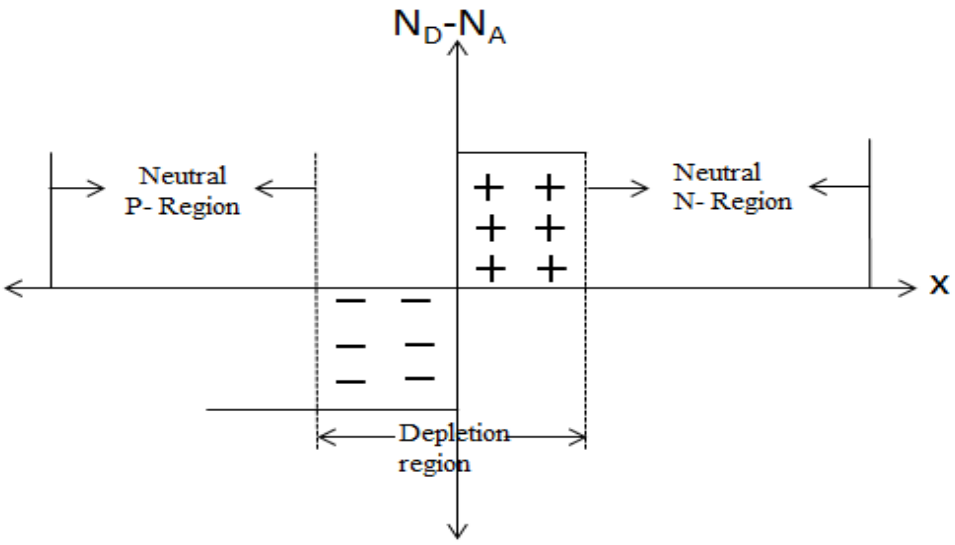

Figure 8 Space charge distribution in an abrupt P-N junction

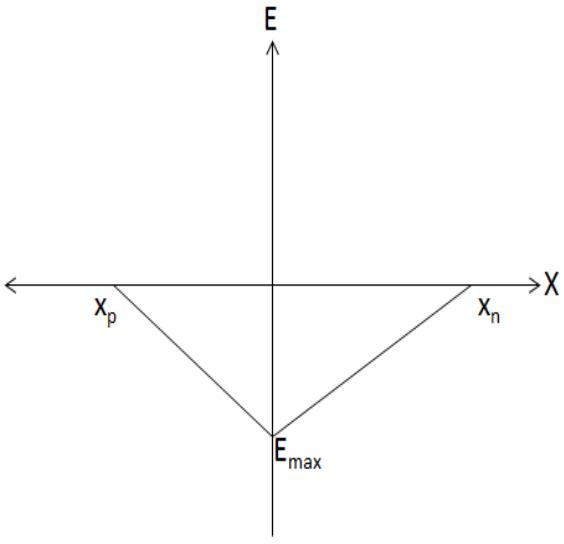

Figure 9 Electric field distribution of an abrupt P-N junction

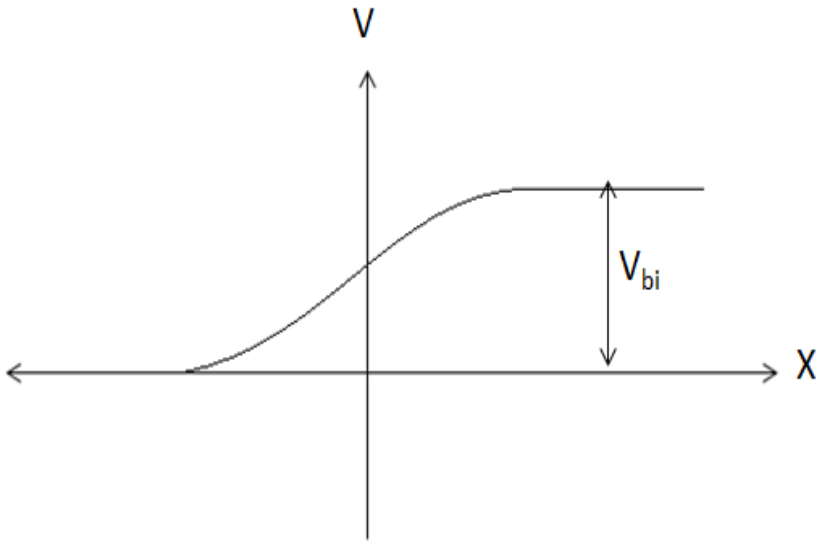

Figure 10 Potential variation of an abrupt P-N junction

In figure 9, X_p refers to the distance of the diffused electrons in the p-region and X_n refers to the distance of the diffused holes in the n-region. E is the electric field, E_{max} is the maximum electric field and the area of $\Delta X_p E_{max} X_n$ is equal to the diffusion potential. In figure 10, V symbolizes the potential and V_{bi} indicates the built in potential.

2.3 Heterojunction

The junction formation between two dissimilar semiconductors is termed as a heterojunction. Figure 11 shows the energy band diagram of two dissimilar semiconductor which are isolated from one another.The band bending in heterojunction is different than homojunction because of the difference in bandgap, electron affinity and work function of the two dissimilar semicondcutors. Figure 12 shows the band diagram after the heterojunction formation. In figure 11 and figure 12, the subscript 1 is assigned to the symbols which describe semiconductor 1(p-type) and the subscript 2 is assigned to the symbols which describe semiconductor 2(n-type). χ represents the electron affinity, Φ is the work function, E_g is the bandgap, ΔE_C and ΔE_V are the

change in conduction and valence band respectively. E_C, E_V and E_F are the conduction band energy, valence band energy and the Fermi energy.

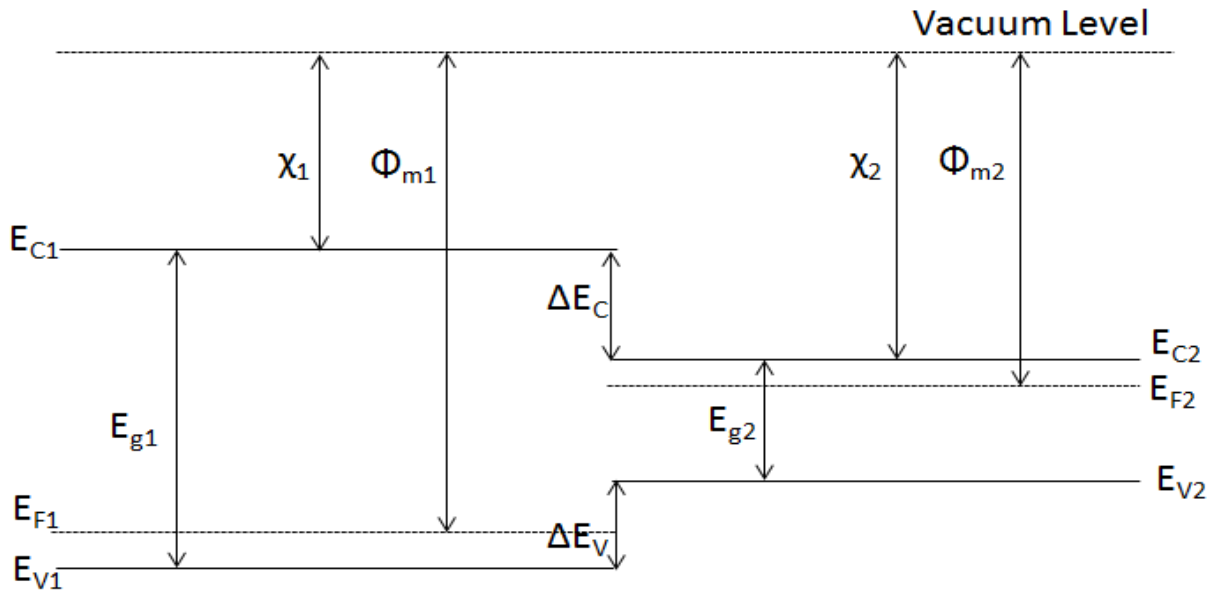

Figure 11 Energy band diagram of two isolated semiconductors

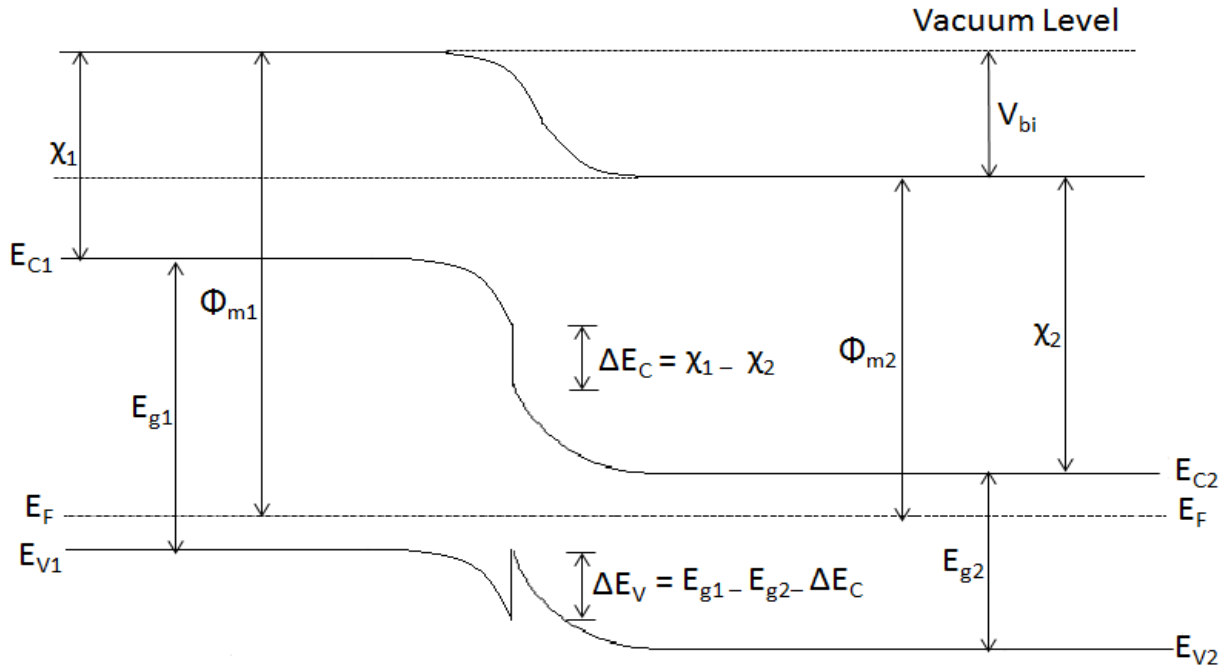

Figure 12 Heterojunction of an ideal P-N heterojunction at thermal equilibrium

We have $E_{g1} > E_{g2}$ and the discontinuities in the band are given by:

$$\Delta E_C = \chi_1 - \chi_2$$

Equation 5 Discontinuity in the conduction band

$$\Delta E_V = E_{g1} - E_{g2} - \Delta E_C$$

Equation 6 Discontinuity in the valence band

Solar cells are preferred to have a heterojunction than a homojunction . The main reasons being:

1. A solar cell must effectively make use of the solar spectrum. The heterojunction has two dissimilar semiconductors having two different bandgaps, E_{g1} and E_{g2} ($E_{g1} > E_{g2}$). If one side of the larger bandgap semiconductor is placed facing the sun and the other side is in a heterojunction contact with the lower bandgap semiconductor, the photons with energy greater than or equal to E_{g1} are absorbed by the top layer and the top layer acts as a window for lower energy photons which are absorbed in the lower bandgap semiconductor. This is not possible in a homojunction because both the semiconductors have the same bandgap.

2. Considering the structure of the solar cell, the P-N junction is followed by the front contacts to tap out the electrons. When the carriers are generated outside the depletion region and if they are more than a diffusion length away, they have a high chance of recombination to the front contact. In a heterojunction, the top wide bandgap layer can be made thin so that most of the light reaches the junction and the lower bandgap material significantly reducing recombination to the front contact. The energy band, conduction band and valence band offsets can be schematically shown for the various junction formations in a solar cell. Wei

and Zunger [13] calculated theoretically the offsets between CGS, CIS and CdS. The offset between CdS and ZnO was calculated more recently [14]. Figure 13 shows the schematic representation of the theoretically determined offsets.

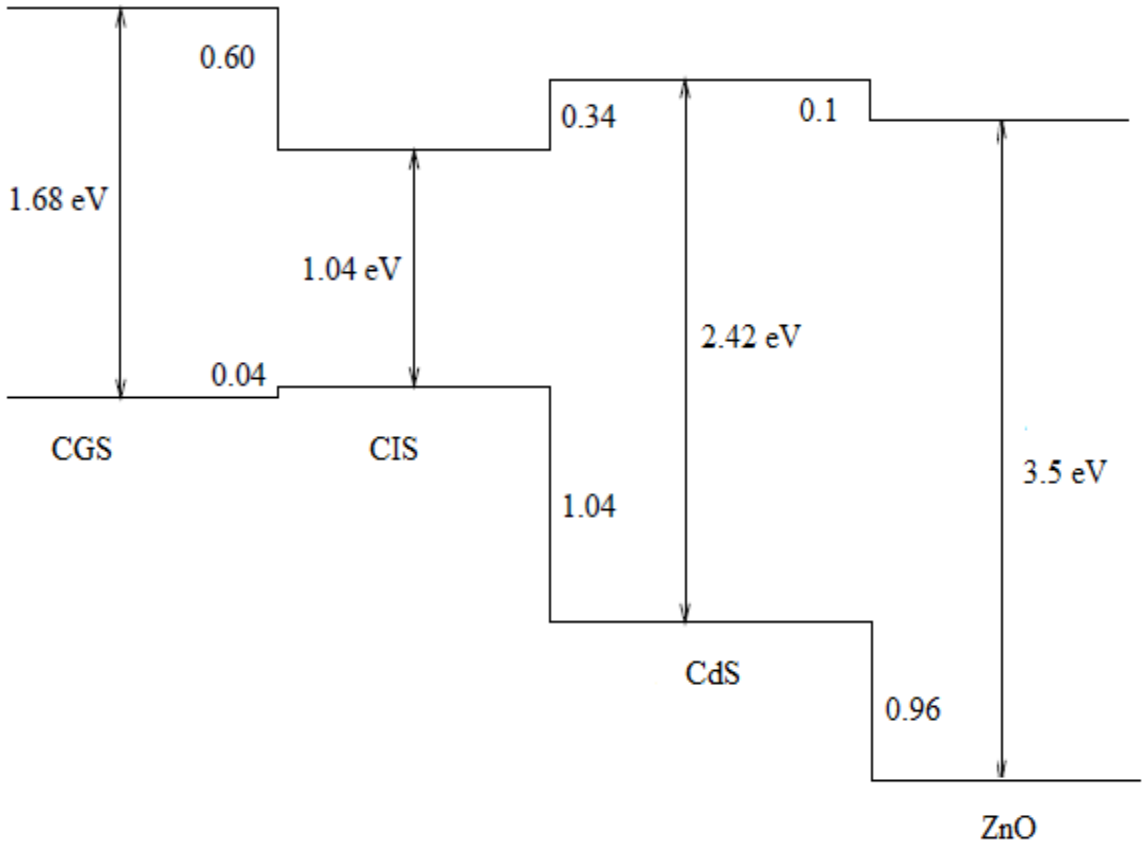

Figure 13 Band offsets between CGS – CIS – CdS – ZnO

As we can see from above figure, the bandgaps of the materials are aligned in such a way that the light is incident on the higest bandgap material first (with the exception of CIS and CGS, this is because we tend to form a Cu rich CGS base for increased grain growth of the subsequent layer), all the high energy photons are absorbed here. The lower energy photons are be absorbed by subsequent layers and hence we can see a decreasing tend in bandgap. The bandgap of CGS and CIS are such that the higher band gap CGS is towards the backside and lower bandgap CIS is

towards the front. This is due to the fact that Ga tends to accumulate towards the back of the device and section 1.5.1 discusses how the bandgap can be engineered by varying the Ga content for improved cell performance.

2.4 Solar Cells

Solar cells are semiconductor devices which convert light to electricity. The semiconductor devices with which solar cells are made consist of a P-N junction. When photons (light) are incident on a material and if their energy is greater than the bandgap of the material, they have sufficient energy to excite electrons to the conduction band.

$$E = hc/\lambda > E_g$$

Equation 7 Photon energy greater than bandgap for conduction

where E is the energy of incoming light, h is the Planck's constant, c is the speed of light; λ is the wavelength of incoming light and E_g is the bandgap of the material. When electrons are in the conduction band, they are free to move within the material. The excitation of an electron also creates a hole in the valence band which is free to move in the valence band of the material. Thus the successful excitation of an electron by a photon creates an electron – hole pair (EHP) which is free to move in the material. When EHP's are within the depletion region of P-N junction, they are swept across the junction due the drift force generated in the depletion region. These carriers are then tapped out by placing metal contacts. The absorption of light by a material is given by the below equation.

$$I(\lambda) = I_0 \exp[-\alpha(\lambda)\, x]$$

Equation 8 Absorption of light [8]

I_0 is the intensity of light, α is the absorption coefficient, λ is the wavelength of light and x is the distance penetration depth of light from the surface of incidence.

2.4.1 Photocurrent Generation and Spectral Response

The solar responds to the different spectrum of the sun in different ways. This means that the amount of photo carriers generated varies for different wavelengths of sunlight. The spectral response of a solar cell gives us an idea about the quantum efficiency of the solar cell. The quantum efficiency of the solar cell tells us the amount of photons that are converted to electrons. Ideally this ratio should be one, but it varies depending on the wavelength of light and bandgap of the material. The rate of generated photo carriers is given by the equation:

$$G(\lambda, x) = \alpha(\lambda)\, F(\lambda)\, [\, 1 - R(\lambda)\,]\, \exp[-\alpha(\lambda)\, x]$$

Equation 9 Generation rate of photo carriers [6]

where $F(\lambda)$ is the number of incident photons per cm^2 per second per unit bandwidth, $R(\lambda)$ is the fraction of these photons reflected from the surface and x is the distance from the surface where EHP's are created. Assuming low injection conditions and necessary boundary conditions, the spectral response is given by the equation:

$$SR(\lambda) = \frac{1}{qF(\lambda)\,[\, 1 - R(\lambda)\,]}\, [\, J_p(\lambda) + J_n(\lambda) + J_{dr}(\lambda)\,]$$

Equation 10 Spectral response

Current density is current per unit area and it is represented by J. $J_p(\lambda)$, $J_n(\lambda)$ and $J_{dr}(\lambda)$ are the photo-current density contributions from p-region, n-region and depletion region respectively. $SR(\lambda)$ is the internal spectral response and q is the charge of an electron. The photocurrent

density can be obtained from the spectral response. If λ_m is the longest wavelength corresponding to the absorber bandgap, the photocurrent density is given by the equation:

$$J_L = q \int_0^{\lambda m} F(\lambda) [\ 1\ -\ R(\lambda)\ ] SR(\lambda)\ d\lambda$$

Equation 11 Photocurrent density

2.4.2 Current-Voltage (I-V) Characteristics

As discussed previously when photon excitation create EHP's near the depletion region, they give rise to the flow of charge carriers. These charge carriers are termed photocurrent. In the dark, the solar cell does not produce any photo current and it is given by the diode equation:

$$I = I_0 (\exp (qV/kT - 1))$$

Equation 12 Dark current of a solar cell [1]

where V is the applied bias, I_0 is the reverse saturation current, k is the Boltzmann constant and T is the absolute temperature. When light is shone on a semiconductor material, photocurrent is generated and it is given by the equation:

$$I = I_0 (\exp (qV/nkT - 1)) - I_L$$

Equation 13 Photocurrent under illumination [1]

where n is the diode ideality factor and I_L is the photo generated current. The short circuit current (I_{sc}) is obtained when no bias is applied to the P-N junction and the open circuit voltage is obtained when I=0. The open circuit voltage is given by:

$$V_{OC} = (kT/q) \ln [(I_L/I_{sat}) + 1]$$

Equation 14 Open circuit voltage [1]

The photo generated current (I_L) is relative to the depletion width (W), minority carriers diffusion length of holes and electrons (L_p and L_n), the area (A) of the active region and the generation rate (G) of EHP's. It is given by:

$$I_L = qAG\ (L_p + L_n\ + W)$$

Equation 15 Photo generated current [1]

The current-voltage (I-V) response to the dark and light is shown in figure 14

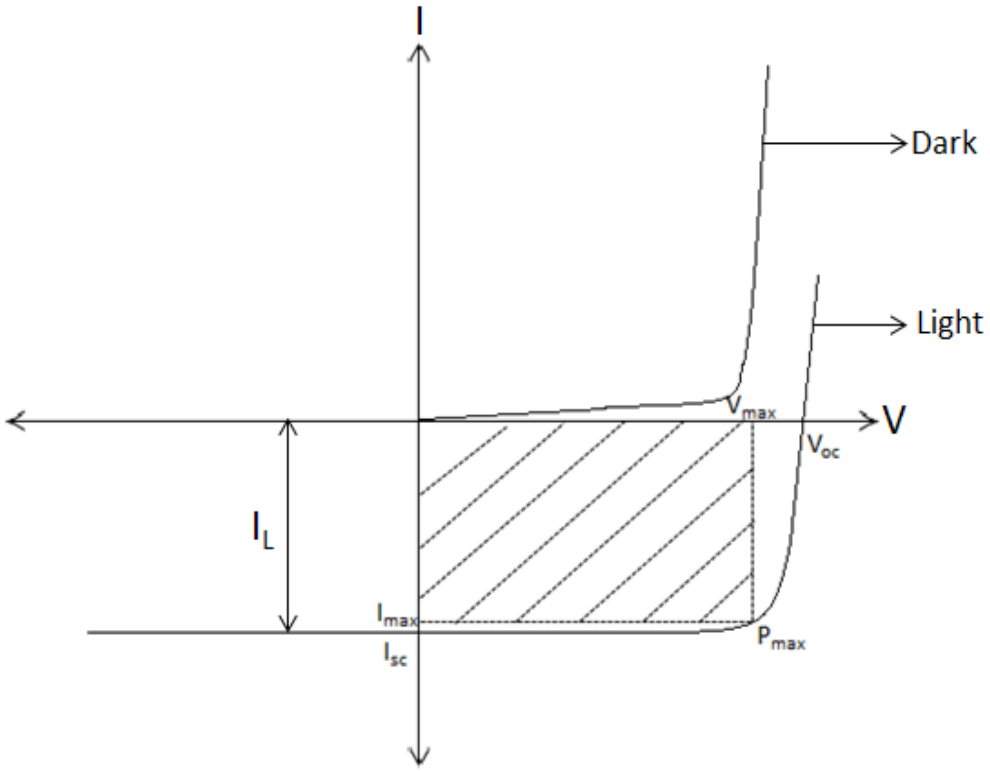

Figure 14 I-V characteristics of a solar cell

As shown in the figure, when the product of current and voltage is positive, as in the first and third quadrants, the solar cell acts a diode. This is analogous to the solar cell in dark. When the product of current and voltage is negative, as in the fourth quadrant, power is generated from

within. This is analogous to solar cell under light illumination. The point of maximum power (P_{max}) is termed as the fill factor. The fill factor is also the product of maximum voltage V_{max} and maximum current I_{max}. It is given by the equation:

$$FF=V_{max}I_{max}/V_{oc}I_{sc}$$

Equation 16 Fill factor [1]

The amount of light that is converted to electricity by the solar cell is given by the efficiency of the solar cell. The efficiency is given by the equation:

$$\eta = P_{max}/P_i = FF\ V_{oc}I_{sc}/P_i$$

Equation 17 Efficiency of a solar cell [1]

P_i is the power of light incident upon a solar cell.

2.4.3 Equivalent Circuit of a Solar Cell

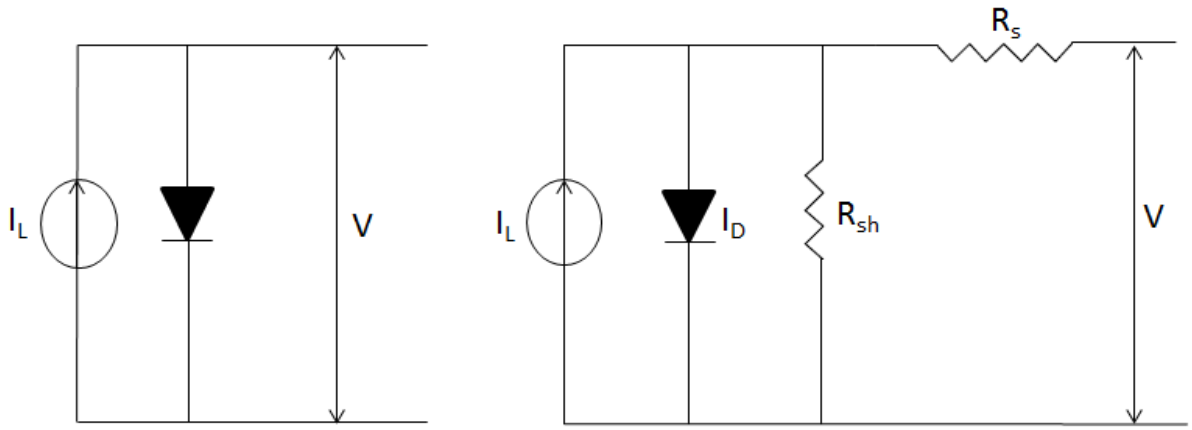

a) **b)**

Figure 15 Equivalent circuit of a solar cell a) Ideal solar cell b) Solar cell with series and parallel resistances

The ideal solar cell and a solar cell with series and parallel resistance is shown in the above figure. An ideal solar cell consist of the photo generated current I_L parallel to the P-N junction, which is represented by the diode. It has infinite shunt resistance and zero series resistance. In reality, solar cells have series and shunt resistances. The series resistance (R_s) has contributes from the bulk resistance of the semiconductor, the metal contacts and also from the contact resistance between the semiconductor and metal contacts. Majority of the series resistance is due to the resistance of the metal contacts. The effect of series resistance on the I-V curve can be seen in figure 16. The effect of R_s can be found from the I-V curve. It is the reciprocal of the slope of the I-V curve under high forward bias. The R_s has no effect on V_{oc} and little effect on I_{sc}, however the FF is significantly reduced.

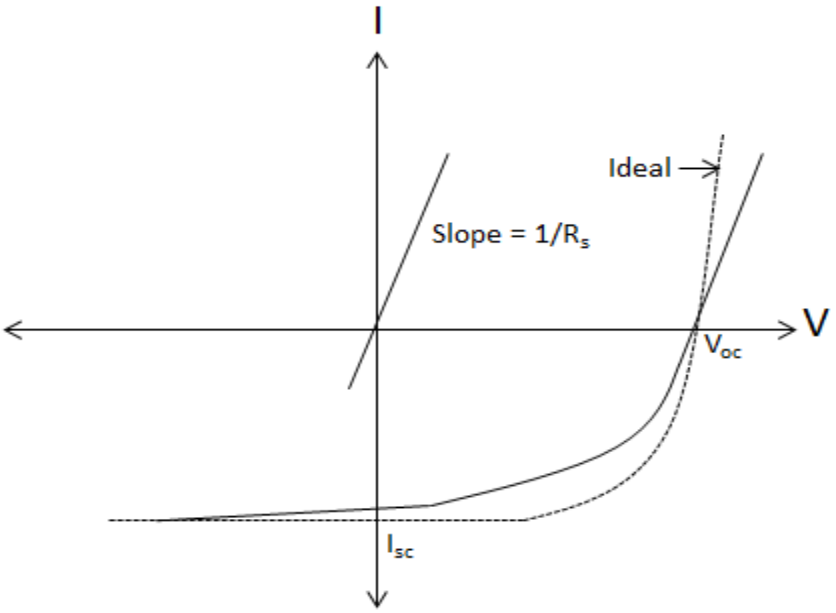

Figure 16 Effect of series resistance

The shunt resistance is mainly attributed to any shorting paths in a solar cell. The presence of pinholes in a solar cell can lead to shorting paths. Figure 17 shows the effect of shunt resistance

on the I-V curve. Shunt resistance is the inverse of slope of the I-V curve under reverse bias. The R_{sh} affects the FF significantly and it als lowers the V_{oc} and current.

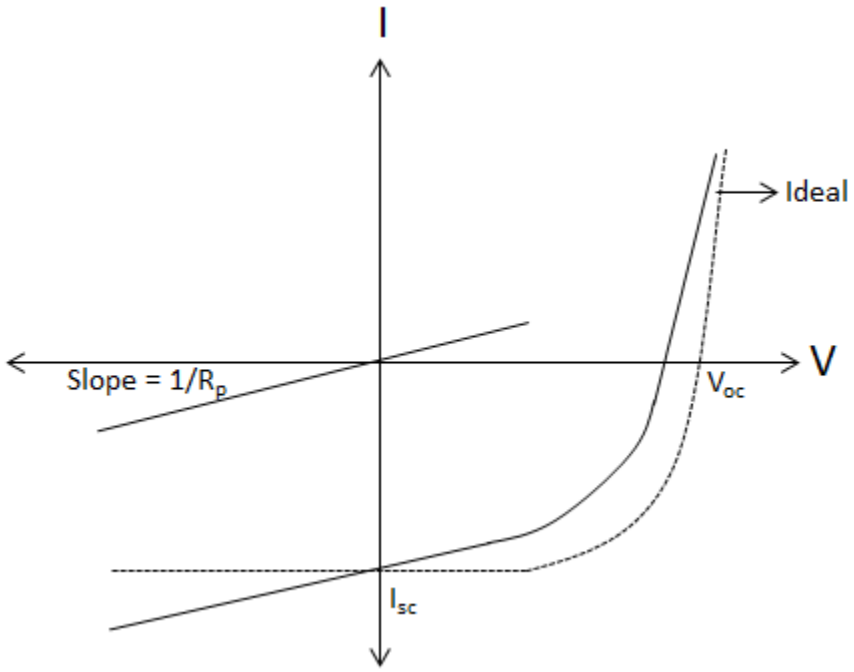

Figure 17 Effect of shunt resistance

CHAPTER 3: DEVICE FABRICATION AND CHARACTERIZATION

This section deals with the device structure and outline followed by the methods used to fabricate them. Our fabricating techniques are clearly explained and the nuances in the characterization methods are also looked upon.

3.1 Device Structure and Outline

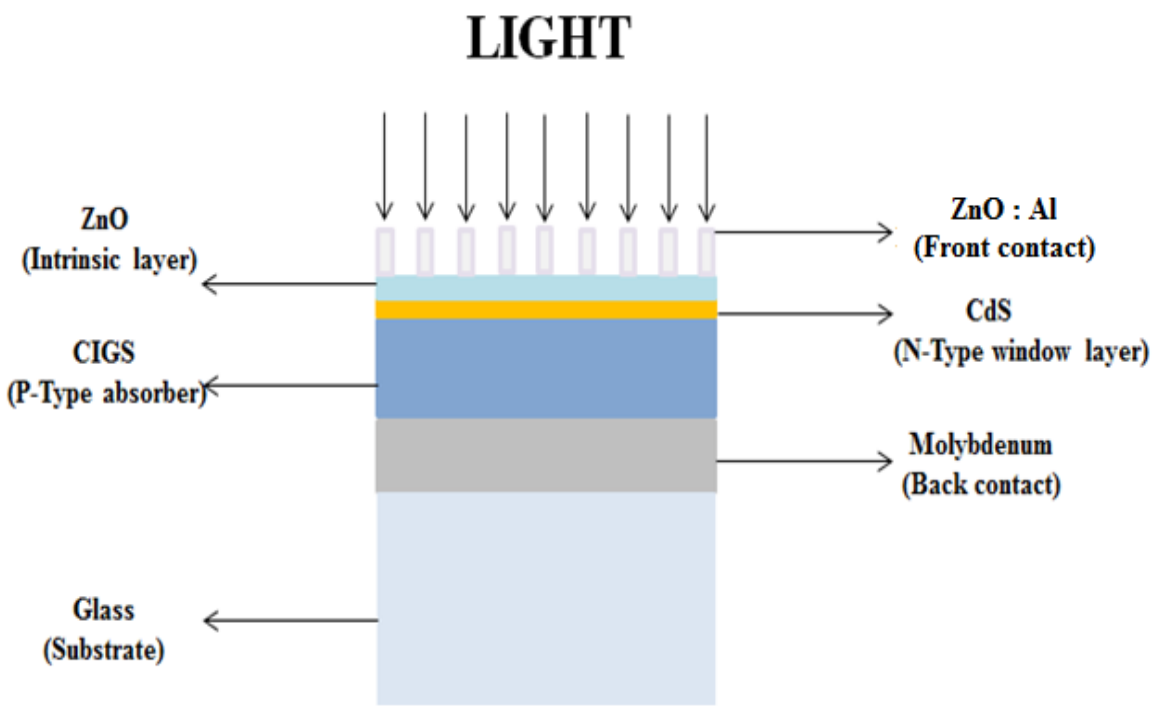

Figure 18 Structure of solar cell

The fabrication of our CIGS solar cells takes shape as shown in the above figure. It's a bottom – up approach done by depositing layers of material over one another. The fabrication of the solar cell is started by depositing materials over a glass substrate. The glass substrate undergoes a

special cleaning procedure (discussed in detail in section 3.2) and then the following depositions follow through:

1. A bi-layer of molybdenum with a thickness of about 1μm. It is deposited by DC sputtering of Molybdenum. This serves as the back contact of the solar cell.
2. 2μm thickness of CIGS. It is deposited by thermal evaporation of Cu, In, Ga and Se sources. This is the absorber layer of the solar cell and it is a P-Type semicondcutor.
3. 800Å of Cadmium sulphide (CdS) deposited by chemical bath deposition of cadmium actetate, thiourea and strong ammonia solution. It acts as the window layer and as N-type semiconductor for the P-N junction.
4. The N-type layer is followed by a 800 Å thickess of ZnO. The ZnO is deposited by RF-sputtering in the presence of argon and oxygen.
5. The final layer of the solar cell is 3000 Å thick aluminum doped ZnO deposited by RF-sputtering in the presence of Ar gas. It is doped with 2% Al. It acts as the front contact of the solar cell.

3.2 Fabrication Techniques

3.2.1 Substrate

The substrate is the base of the solar cell and it should be very clean and smooth. Scratches in the substrate have proven to have negative effects during absorber layer processing [23]. Soda lime glass (SLG) is the substrate used by our group. SLG is preferred due to its low cost and easily availability. SLG is first cut into several 2mm thick square pieces of side 1.34” x 1.34” using a glass cutter. As mentioned earlier (section 1.5.2), the diffusion of sodium from SLG is vital for good device performance. The SLG has a limitation to the maximum temperature it can be

heated. Warps and imperfections were observed in samples when the substrate temperature went above 600°C. SLG is then put to a series of cleaning steps starting with soap scrubbing the glass pieces. Usually a group of ten glass samples were subjected to the cleaning procedure at a time. To minimize damage while scrubbing, we made sure that the teeth of the brush were very soft. The soap scrubbing is done for 3 minutes and after this the individual samples are rinsed under DI water for 2 minutes. After a group of ten samples are scribed and washed, they are place in a holder and put inside a teflon beaker. The beaker is filled with methanol and it is sonicated for an hour. This is believed to remove organics from the glass. After an hour sonication, the methanol is emptied and the samples are washed in DI water again. The beaker is filled with DI water and it is sonicated again for an hour. This makes sure that the glasses are clean from alcohol. The samples are kept immersed in DI water until they are ready for usage. Just before usage, the samples are rinsed once again in running DI water and dry blown with compressed nitrogen. The samples are also slightly heated or kept in the oven for 15 minutes to ensure it is free from moisture before the deposition starts.

3.2.2 Molybdenum Back Contact

Molybdenum is chosen as the back contact because it forms an ohmic contact with the absorber. The deposition chamber is first pumped down to a base pressure of 4μT. It is then purged with Argon gas for the gas to occupy a certain pressure of the chamber. The effect of pressure and power is very critical during the deposition of molybdenum. Films deposited under high power and low pressure are more conductive but have poor adhesion to the SLG as the film is under compressive stress, whereas films deposited under low power and high pressure have better adhesion but poor conductivity as the film is under tensile stress [15]. A bilayer of molybdenum is deposited with the initial layer deposited under high working pressure (10mT) in order to get

good adhesion with SLG and the second layer is deposited at low pressure (4mT) to get good conductivity. A constant power of 860W was used throughout. The rate is kept constant at 12Å/s for the initial layer and 15Å/s for the second layer. The initial layer is 2000Å thick and the second layer is 8000Å thick. Such a bilayer structure is used as the back contact of the solar cell.

3.2.3 CIGS Thermal Evaporator System

The CIGS absorber layer is a P-type semiconductor. Ongoing research and past data from the USF semiconductor laboratory has suggested that the best devices are made with Ga/(In+Ga) ratio close to 0.3 and Cu/(In+Ga) close to 0.9. The CIGS absorber layer fabricated in this thesis deals with a multisource thermal evaporation system. The system has 4 effusion cells each containing the materials copper, indium, gallium and selenium. Each effusion cell has a crystal monitor associated with it to determine the rates at which the elements are deposited. The power controllers heat up the effusion cells, the power is varied based on the feedback from the thermocouple. A set temperature is entered in the power controller and the thermocouple gives the feedback to the power controller based on the temperature of the respective effusion cell. When the set temperature is reached, the feedback makes sure that the effusion cells receive optimum power to maintain the desired temperature. Care should be taken while using a multi-source system for absorber deposition. The wide variety of elements and the long fabrication time used to create the absorber can increase the rate of error inside the chamber. The chamber should be well cleaned from time to time and the effusion cells must be checked for power and thermocouple shorts often. Liquid nitrogen is used as a cold trap, mainly for freezing the Se vapors. This helps to protect the turbo pump during the course of the run. A gate valve is used to divide the chamber into two and a vent valve is used to vent the chamber after the deposition. Figure 19 shows a rough overview of the multisource evaporation chamber.

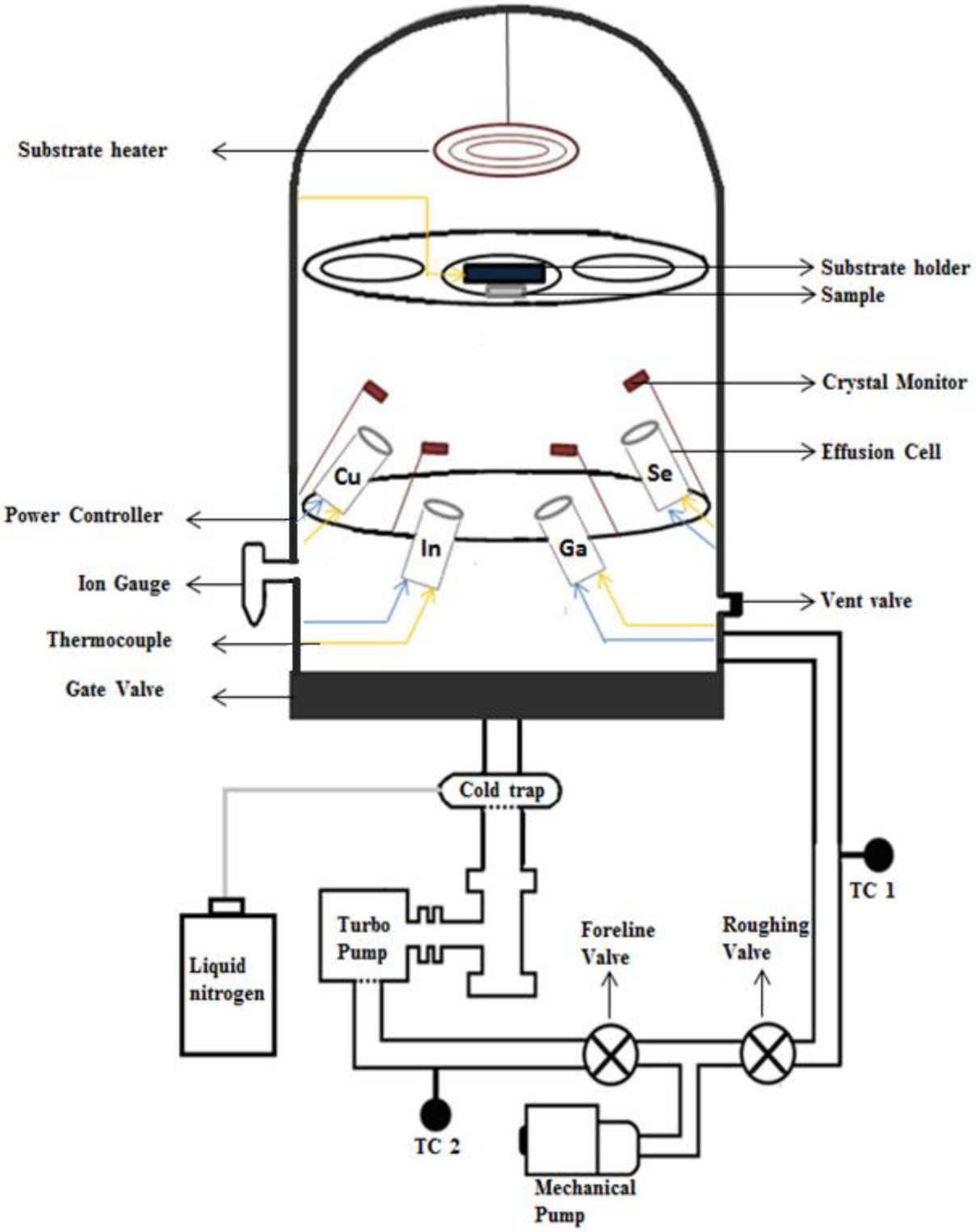

Figure 19 Thermal evaporator used in CIGS growth

A sample is tightened to a sample holder and loaded to the chamber. The thermal evaporator has two pumps to keep it under vacuum. Initially the roughing pump or mechanical pump is used to pump the chamber to a pressure of 90mT. The roughing valve is opened first and this pumps down the section above the gate valve to 90mT. Once this pressure is reached, the roughing valve is switched off and the foreline valve is turned on. The section below the gate valve is then pumped down to 90mT. The pressure readings from the chamber are read by the two thermocouple gauges TC1 and TC2. Once the upper and lower section of the gate valve is of the same pressure (90mT), the gate valve is opened. After the gate valve is opened, the chamber becomes whole instead of two separate sections and the pressure is low enough for the turbo pump to be switched on. The ion gauge is used to read pressures below 1mT. The turbo pump is switched on and the chamber is allowed to pump down to 5μT. This pressure is low enough to have a large mean free path and once this pressure is reached the effusion cells are gradually heated in steps. The substrate heater which is controlled by a variable transformer is also simultaneously ramped up to desirable temperature. In the figure 19, the shutters to individual effusion cells are not shown to avoid complexity of the diagram. Shutters for individual cells can be opened to check if the rates of the materials are as required. There is also a sub shutter which covers the sample and is opened only when the deposition begins. So the need of worry for sample contamination during opening the effusion cell shutters is avoided. The sub shutter is also not shown in fig 19 to avoid complexity of the diagram. Once the effusion cells have reached desired temperature, a program which uses light-o-rama controller to open and close shutters at precise intervals is used to follow a particular time profile for the growth process. The intervals at which these shutters are opened and closed decide the outcome of the deposition. Liquid nitrogen is filled to a tank and it is connected to the chamber through a hose. This set acts as a

cold trap for the system. After the deposition is finished, turbo is switched off, roughing valve and foreline valve are closed and the system is allowed to cool to around 50°C. After the chamber has cooled, the vent valve is opened and the chamber is vented. The sample is now ready for the next step.

3.2.3.1 Fabrication of the CIGS Absorber Layer

The fabrication of the two stage growth recipe starts with the deposition of Copper, Gallium and Selenium. The rate of copper, gallium and selenium are maintained at 2Å/s, 1.5Å/s and 15Å/s respectively. Details regarding the flux rates and order of deposition are mentioned in the results section. The fluxes of copper, gallium and selenium combine together on a molybdenum coated glass substrate, which is placed at an optimum distance from the sources and maintained at 300°C (figure 19). The CGS deposition goes on for the first 34 minutes. During the 27th minute of the CGS deposition, the substrate temperature is increased from 300°C to 550°C and the selenium flux is increased from 15Å/s to 25Å/s. This rise in substrate temperature and selenium flux is done uniformly in a time span of 7 minutes. An increase in the substrate temperature increases the incorporation of Se in a CIGS film [21]. At the 34th minute, the substrate temperature is 550°C and the selenium flux is 25 Å/s, it is at this point indium comes into play and it has a flux rate of 2.5Å/s. The metal fluxes are Cu-2Å/s, In-2.5Å/s and Ga-1Å/s. From this point on, the second stage of deposition takes place till the 56th minute. Thus the second stage of deposition lasts for 22 minutes and the total run time mounds to 56 minutes. At the 56th minute, the metals are switched off, but the Se flux is maintained at 15 Å/s for 10 minutes. This step ensures that there is enough Se flux to maintain the selenization. At the end of the 66th minute, the potentiometer which maintains the substrate temperature at 550°C is turned to zero, and the sample is set to cool to room temperature. As there is a loss of gallium and indium due to the

formation of volatile gallium and indium species [22], the selenium flux is maintained at 5 Å/s until the substrate temperature reaches 225°C. This temperature drop takes about 20 minutes.

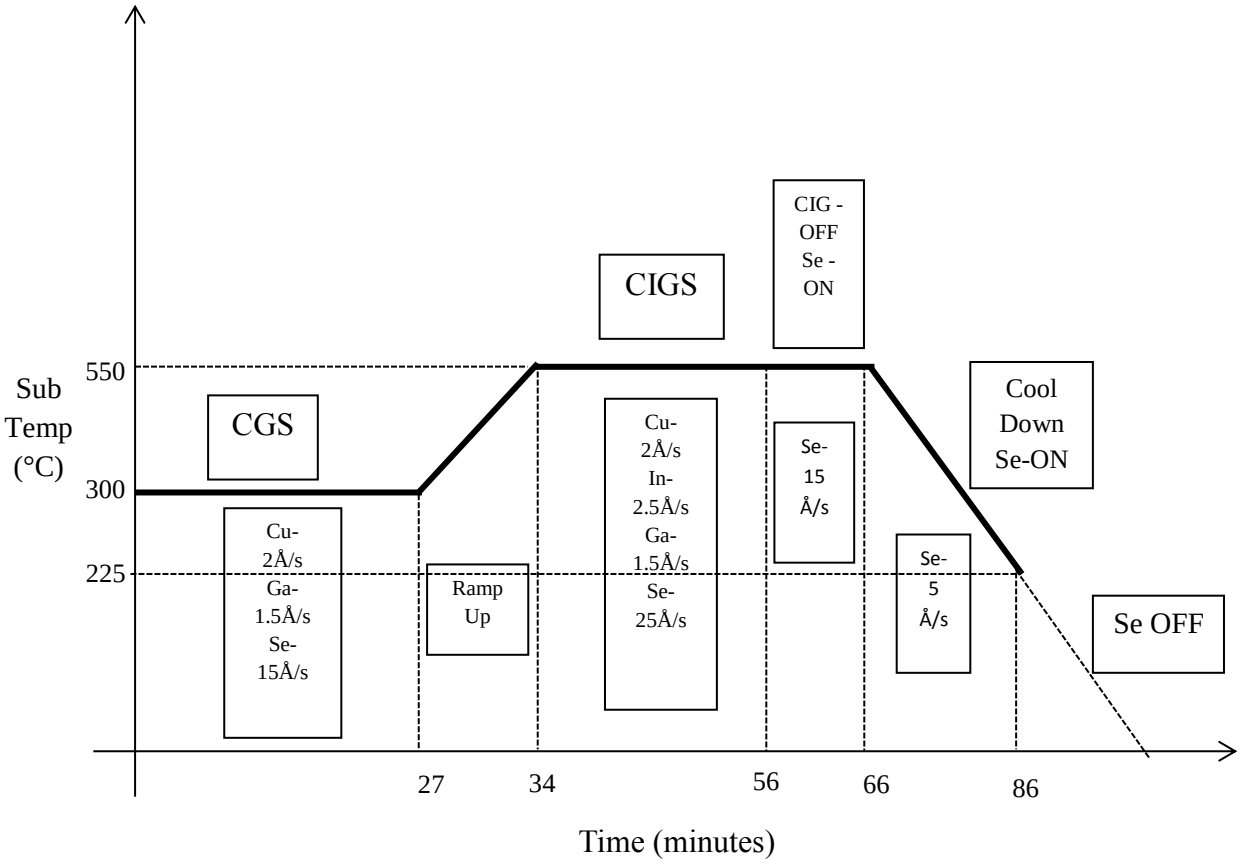

Figure 20 Time-Temperature profile for CIGS absorber layer

3.2.4 Chemical Bath Deposition of the N-type Contact

The CIGS layer is succeeded by the deposition of cadmium sulfide (CdS). CdS has a bandgap of around 2.4eV and the wavelength of sunlight in this region is absorbed by this layer and the wavelength lesser than this bandgap is transmitted through the layer. CdS is deposited by chemical bath deposition of cadmium acetate, thiourea and strong ammonia solution. The process is as follows: A beaker is filled with 400ml DI water. After the deposition of absorber

layer, the sample is kept under vacuum until the sample is ready for the CdS deposition. The sample is taken out just before the CdS deposition and it is immediately placed in a sample holder and put into the beaker filled with DI water. A magnetic stirrer is placed below the sample holder. 60ml of 0.15M cadmium acetate and 75ml of strong ammonia solution is poured into the beaker filled with DI water. This setup is the placed in a hotplate and a predetermined heating rate is set and the magnetic stirrer is made to spin. Once the heating and stirring starts, a thermometer is inserted inside the beaker to note the temperature of the solution. When the temperature reaches 30°C, 60ml of 0.15M thiourea is added to the solution. The solution is heated until 80°C and then it is timed to about 1 minute and 30 seconds. Since a lot of parameters are associated with the procedure a proper understanding of the precipitation process and the color change of the solution is required to know if a proper deposition has taken place. Once the sample holder is taken out of the solution, it is transferred to another beaker containing DI water and allowed to cool for 5 minutes. Once this is done, the water containing impurities is poured and new DI water is filled in. The beaker is set to sonicate for 15 minutes [16]. It is also proven to produce uniform films under non optimal conditions (excess or shortage of precursor concentrations). The sample is now ready for the subsequent intrinsic layer and top contacts.

3.2.5 ZnO Deposition

The intrinsic ZnO is deposited after the CdS deposition and before the front contact. The role of ZnO is to act as a buffer layer. It is called as the buffer layer because it protects the sensitive absorber layer from damage during subsequent processing of other layers. For example, our procedure follows the deposition of aluminium doped zinc oxide (ZnO:Al) by RF sputtering after the ZnO deposition. If this deposition had taken place before the buffer layer growth, it would have damaged the absorber layer. ZnO is deposited by RF sputtering. 800Å of ZnO is deposited

in an atmosphere of argon and oxygen. The sample is slightly heated before the deposition to drive off any moisture on the substrate. The power of the sputtering gun is maintained at 330W and the rate of deposition is maintained at 2Å/s. It also serves as a barrier to the aluminium atoms of the succeeding front contact layer. This barrier stops the Al atoms from diffusing into the CdS layer and causing a short.

3.2.6 Front Contact ZnO:Al Deposition

The front contact is contains a layer of ZnO doped with aluminium. It is deposited by RF sputtering of ZnO:Al target. Before the ZnO:Al deposition, a mask containing 10 dots (each of 1cm^2 area) is placed onto the predecessor layer of i-ZnO. The device is then loaded into the chamber and the deposition is done. A ZnO:Al layer, which is 3500Å thick is deposited at the rate of 10 Å/s and a temperature of around 125℃. The power of the sputtering gun is maintained constantly at 330W. The electrical and optical properties of this layer are essential to the current produced in a solar cell. The resistivity is expected to be in the higher 10^{-4} region and optical transmission of 90% of the sunlight is expected. Degradation of the target dopants can cause a dip in the electrical and optical properties of ZnO:Al layer which might have a negative impact on the current produced by the solar cell.

3.3 Characterization of the Device

3.3.1 Energy Dispersive Spectroscopy (EDS)

EDS is a technique which uses electron beams to excite the emission of characteristic x-rays from a sample. This technique has a lot of nuances associated with it. The solar cells characterized by our EDS quantitative technique are bound to have a small errors associated with quantitative analysis. One of the most important criteria for EDS quantitative analysis is that the sample should be homogenous. The procedure used to fabricate our absorber layers makes it

non-homogenous. We use a two layer fabrication method, each layer having a different stoichiometry from the other. An EDS performed after the two layer fabrication will be semi quantitative. Another factor involved with the EDS quantitative analysis is the depth from which characteristic x-rays are excited. The depth from which the x-rays are emitted depends on the beam current and the thickness of the sample. If the sample is too thin, the x-rays generated from the bulk might not be very accurate. Thus, an analysis done on the sample should ensure that the sample is homogenous, thick enough for X-rays to pass through the bulk and should also have a smooth surface, which helps in eliminating topographic error. Figure 21 shows the diagram of electron-sample interaction which takes place during EDS analysis. The characteristic x-rays are used to analyze the sample qualitatively and quantitatively.

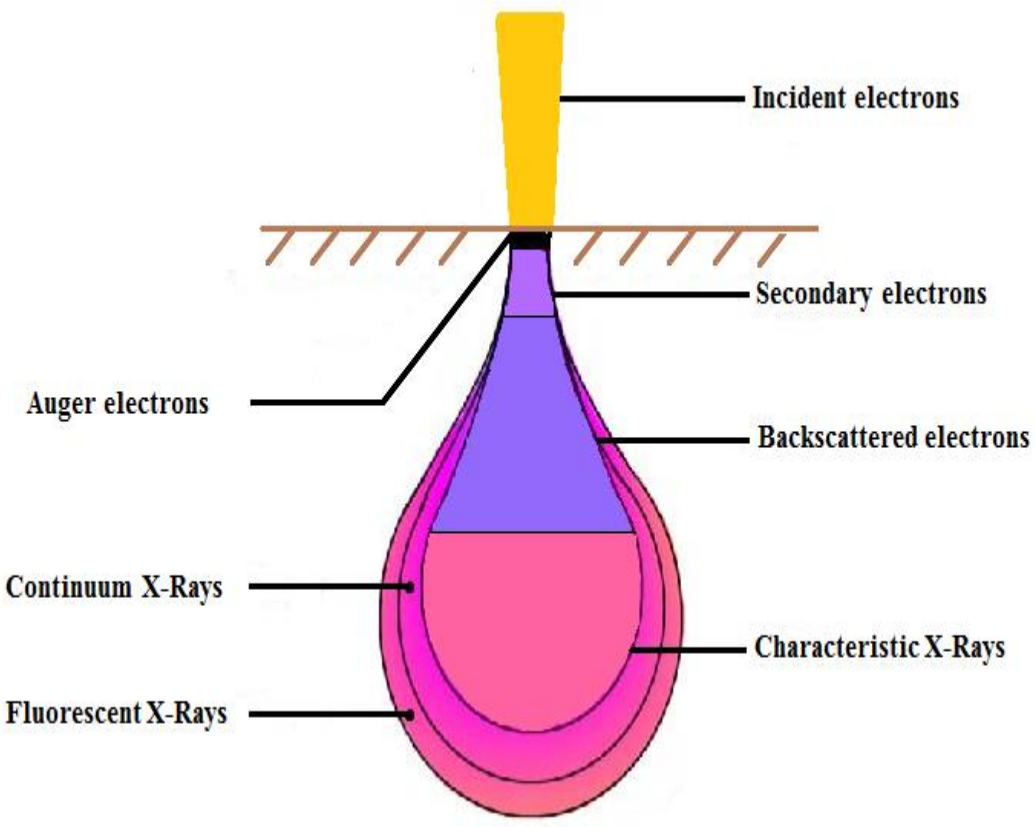

Figure 21 Electron beam - Sample interaction

There are some complications associated with characterizing samples before CdS deposition. An EDS performed before the CdS deposition might cause harm to the absorber layer. It is not advisable to expose the absorber to the atmosphere for a long time as well. Chances of oxygen and water vapor accumulation are more when the sample is used for analysis and this does not go well during the subsequent CdS deposition.

3.3.2 I-V Characteristics

The solar cells were subjected to current-voltage measurements in the dark and light. The curves and plots obtained from dark and light measurements were analyzed. The variation in efficiency was compared to the position and the stoichiometry at that position.

CHAPTER 4: RESULTS AND DISCUSSION

The credit behind the growth recipe goes to the research activities conducted in our lab so far. We have found a way to reduce the cost of CIGS manufacturing using an advancement of the two-stage process. The research looks promising, but the poor reproducibility of results makes it a daunting task for up scaling the process. Errors associated with a multistage evaporation system, improper sample cleaning and storage and nuances in chemical bath deposition techniques are the leading causes associated with poor reproducibility. The results of the device are reproducible after the errors were culminated.

4.1 Two-Step Growth Recipe

The two step growth recipe involves the deposition of Copper Gallium Selenide (CGS) followed by Coppper Indium Gallium di Selenide (CIGS). This may come as a surprise as the bandgap of CGS (~1.68eV) is higher than the bandgap of CIGS (~1.18eV). The reason why CGS is deposited initially is because it provides a growth base for the deposition of CIGS. A copper rich CGS will provide the subsequent layer of CIGS with a larger grain size. Materials deposited at different times throughout the growth cycle are preferred to single stage co-deposition [17]. There is little scope of improvisation in a co-deposition process, whereas materials deposited at a particular time, can make use of certain advantages present at that time. Selenium incorporation in CIGS film is vital to the device performance. Selenium incorporation is almost 50-60% for a wide range of selenium to metal ratios. At low selenium flux, there may be loss of copper [18]. This is a menace, especially when we are trying to get a copper rich CGS base. Thus a low

selenium flux will deter a copper rich base and reduce device performance. It is very important to keep the Selenium to metal flux ratio at 3-5. Figure 22 shows the metal ratio present with respect to the atomic % of Se. These data points were obtained as a result of series of runs which had varying selenium fluxes. The Se fluxes were unmonitored during the course of the run and the varying data supports the fact that the process was not reproducible due to uncontrolled Se flux rate. Under conditions that give rise to excessive Se incorporation there is apparent loss of Ga as well.

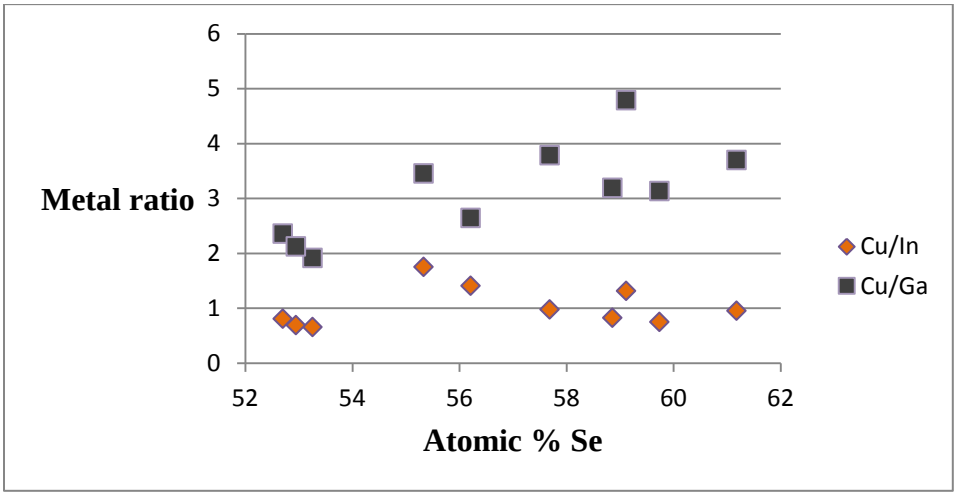

Figure 22 Cu/In and Cu/Ga as a function of Se content

4.2 Controlled Selenium Flux

The two stage process takes place in a chamber with four effusion cells, one each for copper, indium, gallium and selenium. The metals which include copper, indium and gallium, have an evaporation rate which is linearly proportional to temperature. After reaching their evaporation temperature, their flux rate increases at a constant rate with rise in temperature. Thus the metals practically require no monitoring; they just have to be kept at a constant temperature to provide the necessary flux. Selenium on the other hand, is very difficult to control. Once the evaporation temperature is reached, even a small increase in temperature will render the selenium flux

uncontrolled. Once selenium reaches its evaporation temperature its flux rate increases exponentially with rise in temperature. Unmonitored selenium fluxes usually disrupt reproducibility and throw off the stoichiometry. Figure 24 shows the atomic percentage of selenium for eight different depositions, four which were done when the selenium flux was not monitored and four which had their flux rate monitored. The metal ratios of the unmonitored Se fluxes were inconsistent but we can see that the monitored Se flux runs had reproducible results. We can also see that the incorporated Se for the monitored deposition is 60% (which is too high); this needs to be 50 %. This can be achieved by reducing the flux rate of Se.

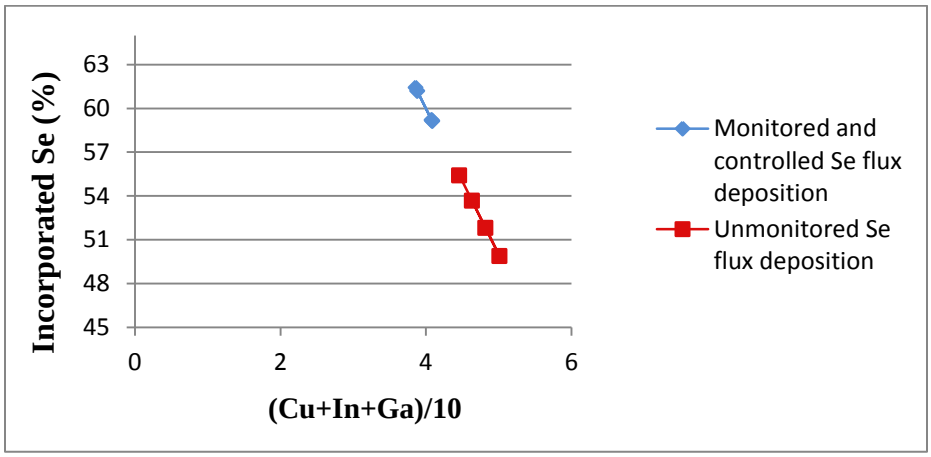

Figure 23 Monitored vs Unmonitored Se flux depositions

4.3 Growth Recipe Changes

The previous two stage growth recipe developed in our lab was poor in stoichiometry reproducibility. This was due to the fact that selenium received the same treatment as the metals, with respect to heating and maintaining a fixed temperature to get a constant evaporation rate. The assumption was that all the elements had a constant flux rate for a fixed temperature. This assumption proved to be costly in terms of reproducibility. There was no fixed Se temperature to maintain a constant flux rate. This is attributed to the ongoing formation of secondary thermocouple effects under the effusion cell. When the Se flux was better monitored, meaning a

certain amount of power was given to maintain a constant flux rate, the growth recipe needed certain changes. The usual growth recipe had the CGS deposition for 29 minutes and CIGS deposition for 22 minutes, Cu was shut off 5 minutes before the total deposition time of 56 minutes. The Cu cut off towards the end was done to maintain stoichiometry. This growth recipe apart from imitating the three stage deposition also proved to disrupt the metal ratios when a constant selenium flux of 25 Å/s was maintained. Series of runs were done to find the right combination. The initial CGS deposition was cut off by 5 minutes, making the first stage of deposition close to 24 minutes and the second stage of CIGS deposition was made to run for 27 minutes taking the total run time to 56 minutes, a constant selenium flux of 25 Å/s was maintained throughout. Let this be called as process 1. Figure 24 shows the Cu/In and Cu/Ga ratios for process 1. The results of process 1 were reproducible, but we were using selenium flux in excess. Few more changes to the growth recipe were done to reduce selenium wastage and get the optimum ratios. Instead of constantly maintaining the selenium flux at 25 Å/s, we maintained selenium to metal flux ratio of 5. The initial CGS run had a selenium flux of 15 Å/s and the subsequent CIGS run had a flux of 25 Å/s, thus avoiding wastage of selenium without compromise in quality. This is called process 2.

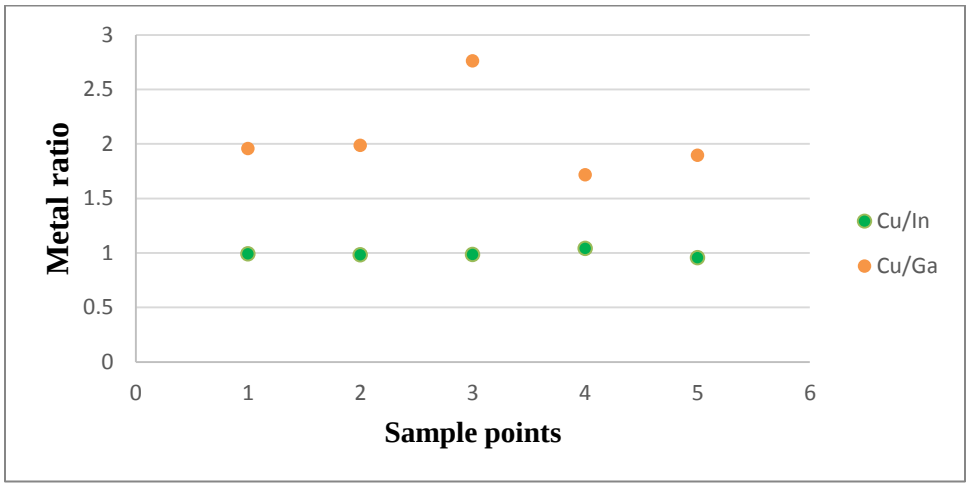

Figure 24 Growth recipe results for process 1

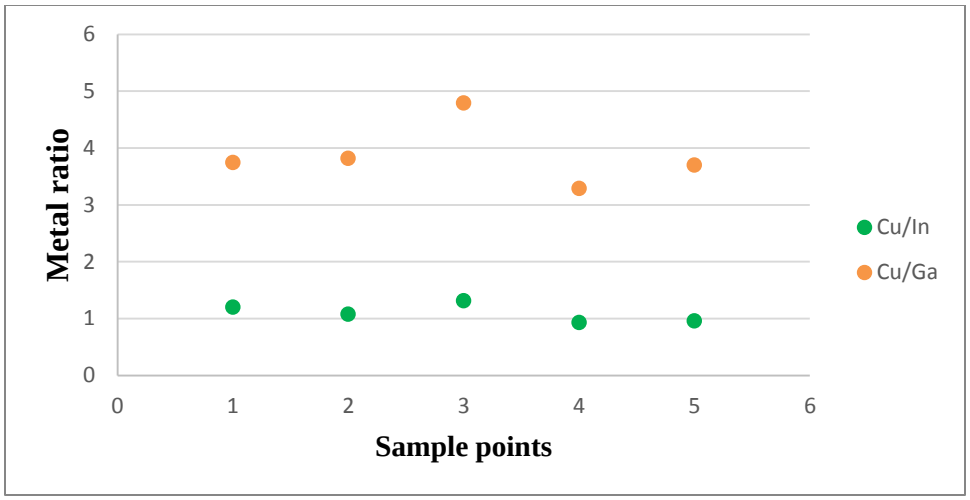

Figure 25 Growth recipe results for process 2

Figure 26 shows the Cu/In and Cu/Ga ratio in process 2. Figure 24 and figure 25 show a few deviations in the Cu/Ga ratios .These deviations are due to gradients found along the sample. These gradients are an outcome of variation in elemental thickness (discussed in section 4.5). Figure 28 shows the metal to group III ratios for process 2. The values of the metal to group III ratios determine the quality of the device. A Cu/III ratio of (0.9 - 1) and a Ga/III ratio of (0.2 - 0.3) are expected for a good device.

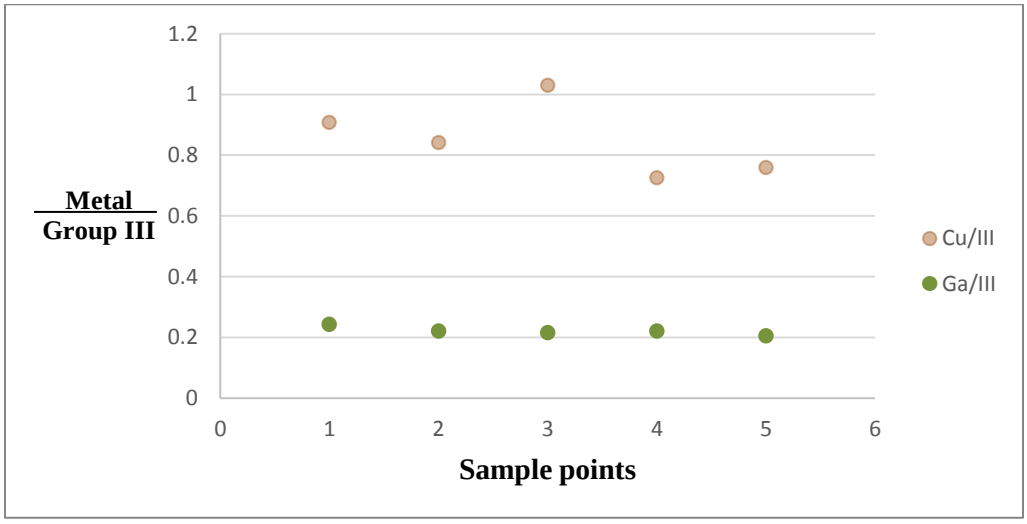

Figure 26 Metal/III ratios for process 2

The copper cut off time was adjusted so that all the elements were shut at the 56th minute, making it an ideal two stage process. This also proved to be helpful for increasing the Cu content in process 2, as a majority of the Cu/III points were below 0.9. This growth recipe has a CGS deposition for the first 34 minutes and followed by a CIGS deposition for the next 22 minutes. The Cu cut off time was slowly increased over the processes to make sure Cu shuts off towards the end of the run. Figure 27 shows how the Cu/III ratio keeps increasing as a result of constant Se flux and increasing Cu cut off time. The run is engineered to get a Cu/III ratio of 0.9-1 and a Ga/III ratio of 0.2-0.3.

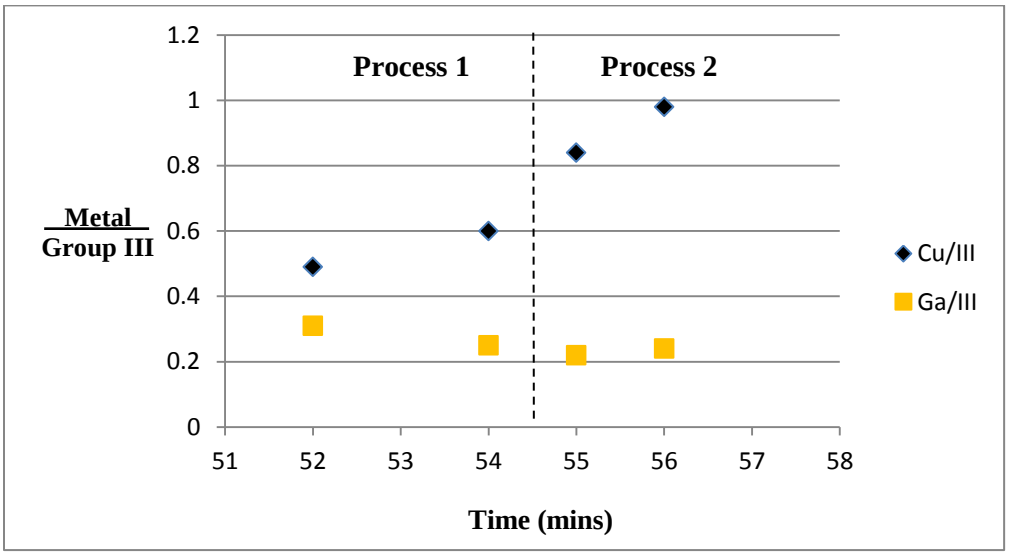

Figure 27 Copper cut off time

4.4 Effect of Growth Recipe Changes

There are a few effects as a result of growth recipe change from an indium cut off time at 24th minute which also has a constant selenium flux of 25 Å/s to an indium cut off time at the 34th minute which has constant selenium to metal flux ratio of 5. The tradeoff between materials for process 1 and process 2 can be seen in the comparison chart of figure 28. The background of the

growth recipe change was to reduce selenium wastage and increase the atomic percentage of copper, overall increasing the copper to group III ratio. By introducing the indium lately, we hoped to bring down the indium atomic percentage and increase the copper by a few atomic percentages. The unexpected act was how gallium reacted to the growth recipe change. For the same gallium rate, a fall in gallium content by a factor of 2/5 was observed, indicating a gallium loss of 40%. We also observed a fall in selenium atomic percentages. It is well understood that the there is more time of CGS deposition for a late introduction of indium. For a CGS deposition, selenium must form various compounds with copper and gallium. The loss of gallium points to the direction of the formation of volatile gallium (Ga_xSe_y). Even though there is a fall in gallium content, the rate of gallium deposition is same in both the growth recipes (process 1 and process 2), meaning the amount of gallium used up in the process is the same. The gallium incorporation has a loss of 40% and this is not a major concern because the Ga/III ratio is brought down from 0.34 to 0.24. The Ga/III ratio was high in the first place and bringing it down only adds more sense to the process.

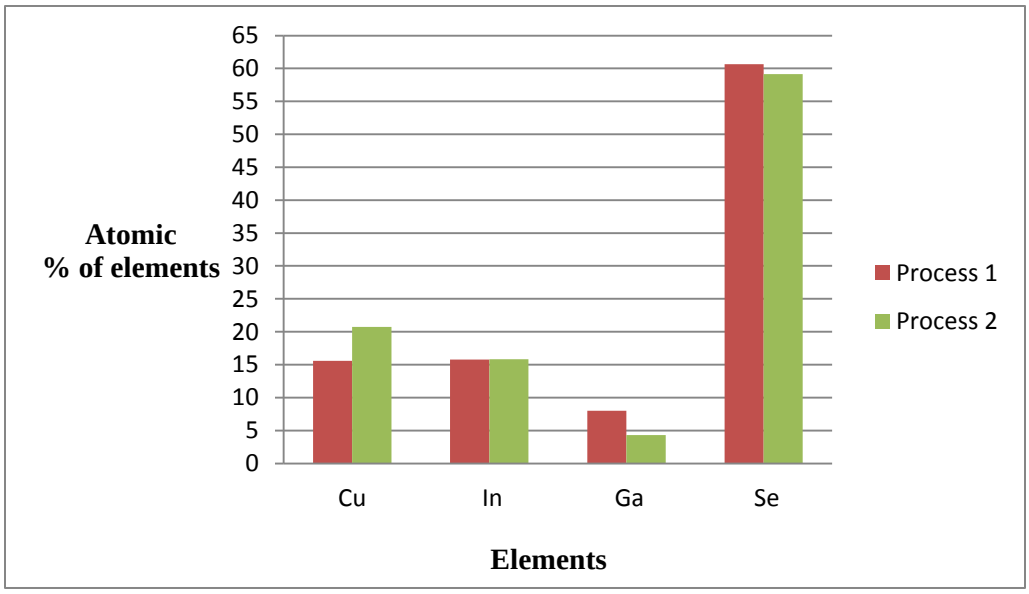

Figure 28 Atomic % of elements present in process 1 and process 2

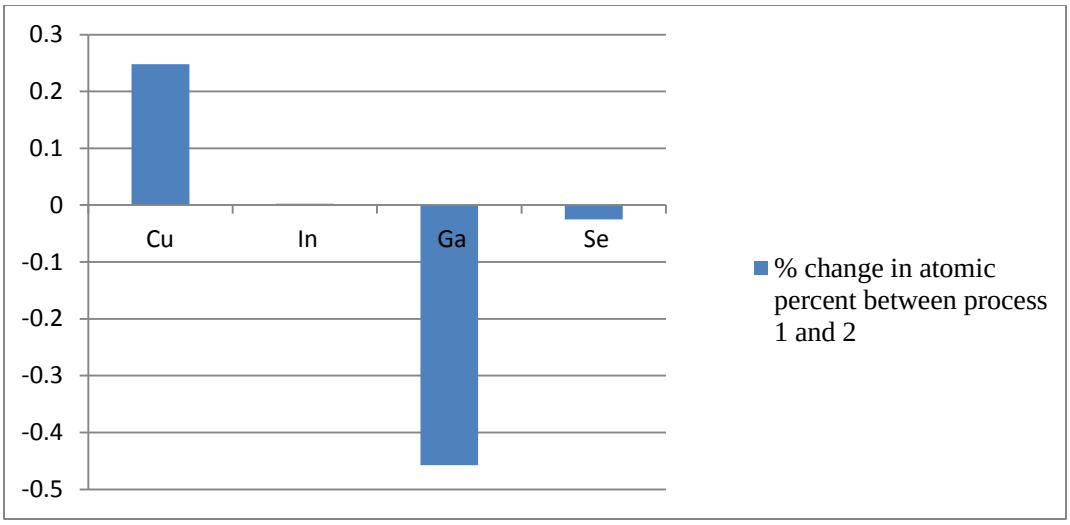

Figure 29 % change in atomic percentage of elements between process 1 and process 2

Figure 29 shows the percentage change in atomic percent of elements between process 1 and process 2. We can see a 24% increase in Cu, an unchanged In, a 47% decline in the Ga content and a 3% fall in the Se content. The shift in process has a profound effect on Cu and Ga.

4.5 Gradients along the Sample

After the absorber deposition, there were a few gradients observed across the sample. These gradients are due to the thickness variation of the elements along the sample. These gradients often interfere with the elemental ratios across the sample. Thus a recipe prepared for an optimum CIGS solar cell might not be the yield the same device performance throughout the sample. An example of atomic composition for a good efficiency CIGS solar cell (SC-47) is shown in figure 30. The orientation of copper and selenium effusion cells are such that they are at the extremes and tilted more than the other effusion cells (figure 19). The thickness variation of copper and selenium across the sample was studied. For testing the thickness of elements, a kapton tape was used and a timed deposition of the element was done. After the deposition, the tape was removed and a profilometer was used to measure the step height. Figure 31 shows the thickness variation of copper and selenium across the sample. Point 2 in Se thickness is prone to

a minor error for the huge variation it shows. The error can be due to the fact that kapton tape was placed, peeled and replaced on the sample. As a result of this there were glue deposits from the kapton tape. This might have caused a minor error during the step height measurement. The figure shows that copper is pretty stable throughout the sample but selenium has a lot of variations. The high flux rate of selenium can contribute to the non-uniform thickness across sample. Figure 32 shows the variation of device performance with variation in stoichiometry.

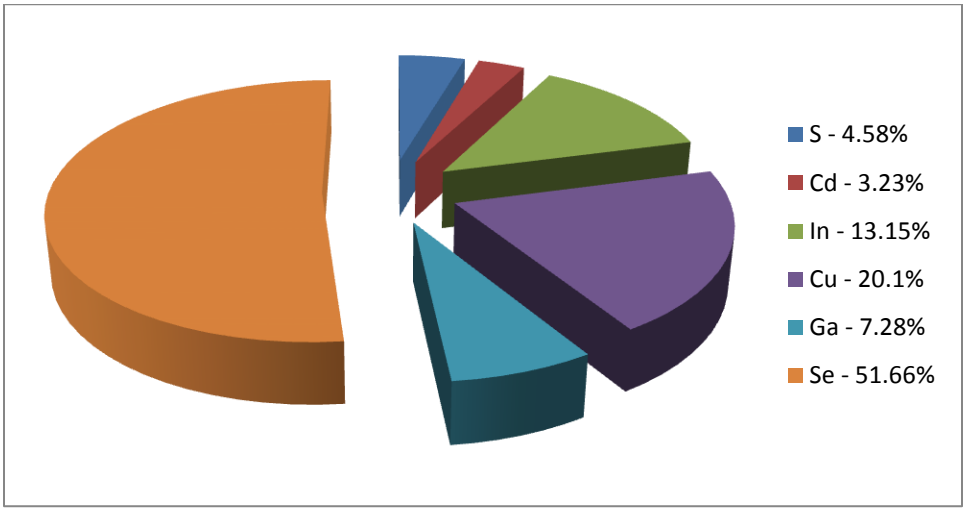

Figure 30 Atomic composition of elements for SC-47

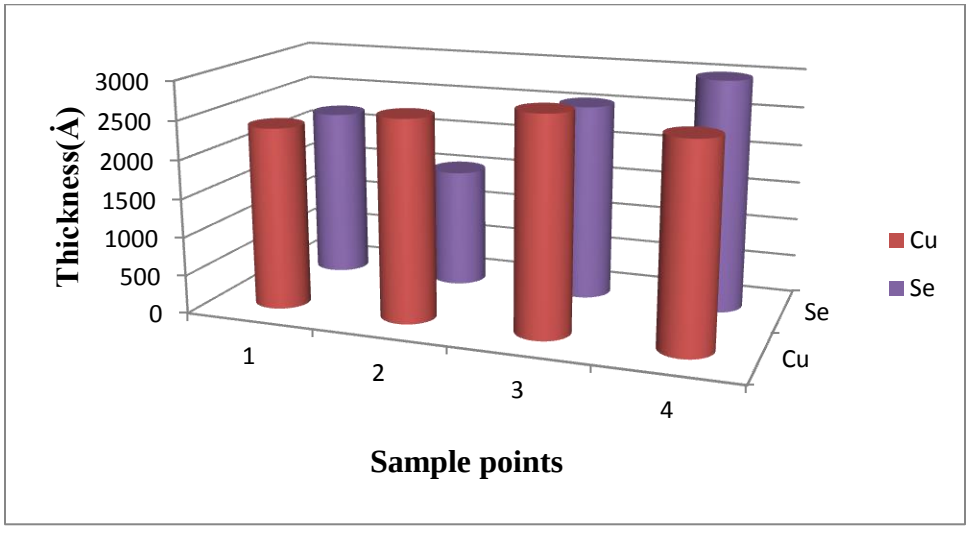

Figure 31 Thickness variation across the sample

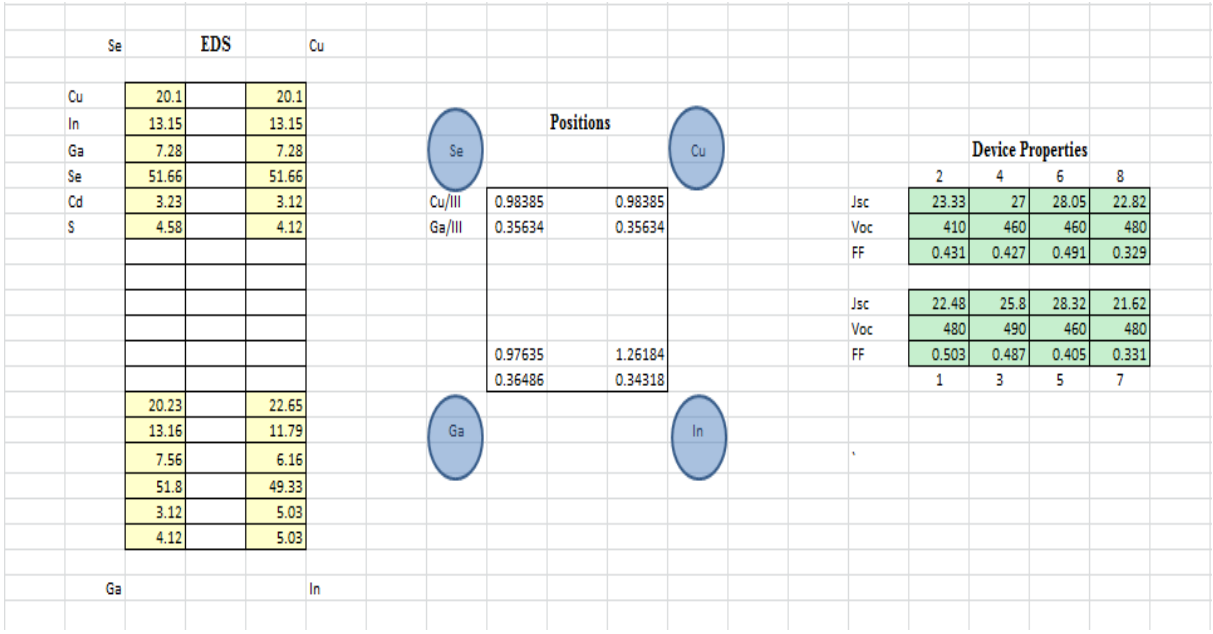

Figure 32 Device performance as a result of thickness variation

As mentioned previously, an EDS measurement done after the deposition of cadmium sulphide tends to deviate from the normal readings a little. This can be seen in figure 32, where a Cu/III ratio of 1.2 has good device properties, but in reality a Cu/III ratio of 1.2 should not yield working results.

4.6 Improper Sample Storage and Cleaning Process

Glass samples are transformed to solar cells with subsequent thin film depositions. These glass samples must have a proper storage and cleaning process. Molybdenum back contact and the CIGS absorber layer are very sensitive to the cleaning and storing process. Glass samples should never be stored in polymers. The usage of polymers to store samples might lead to sample contamination. When we used polymers to store samples, we found that our subsequent back contact deposition was not adhesive to the glass sample. Instead of recognizing this as an issue with sample storage, we thought our cleaning process was not good enough and we introduced Hydrogen Fluoride (HF) treatment to the cleaning process. Although the adhesion issue was solved using this step, the device performance was on the decline side. The reason HF treatment

was able to solve the adhesion issue was because HF was able to etch away the polymers sticking to the glass substrate. HF was instrumental in getting a proper molybdenum back contact deposition, but we found that it also dissolved the sodium in the soda lime glass. With this happening, there will be no sodium available for diffusion during the CIGS growth process.. This was partly believed to degrade device performance. We finally identified issues with polymer storage and HF treatment and got rid of both the parameters. There was a good adhesion between glass and molybdenum back contact after the polymer storage was stopped, even without the HF treatment. Care should be taken while cutting the soda lime glass into smaller pieces using a glass cutter. Small glass debris and impurities flying around during the cutting process should be immediately washed. Cutting a bunch of samples together, without washing the individual glass pieces immediately, will allow the impurities to dry.

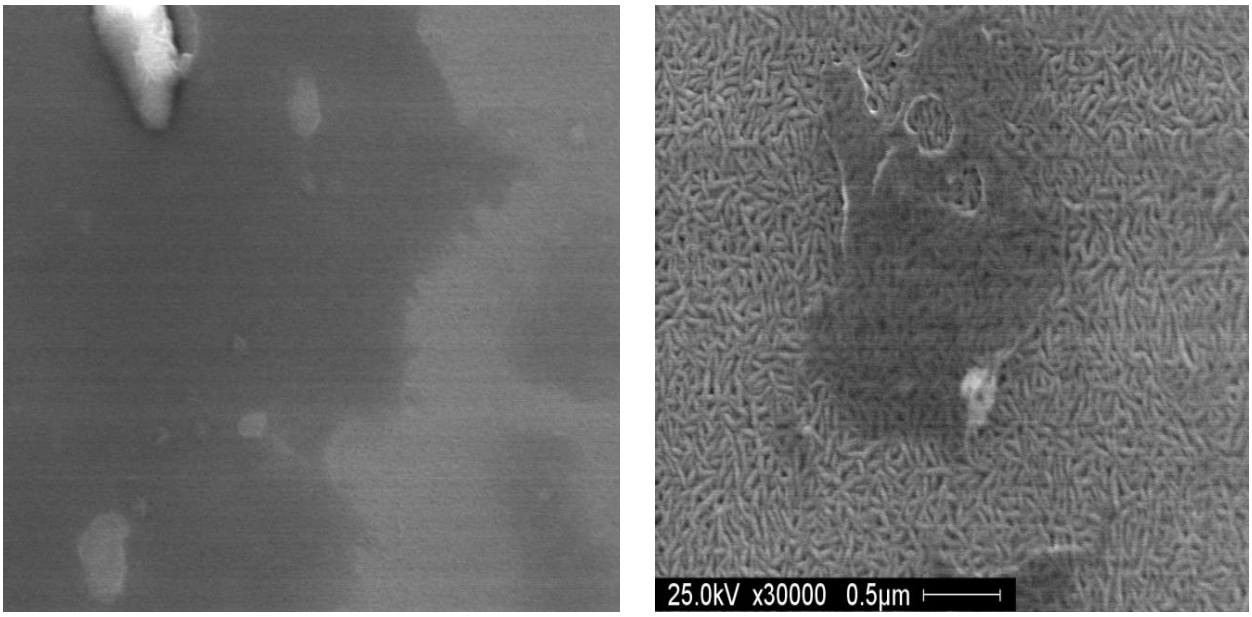

a) **b)**

Figure 33 SEM images of molybdenum a) Gradients observed due to polymer storage b) Contamination observed at 30000X due to polymer storage

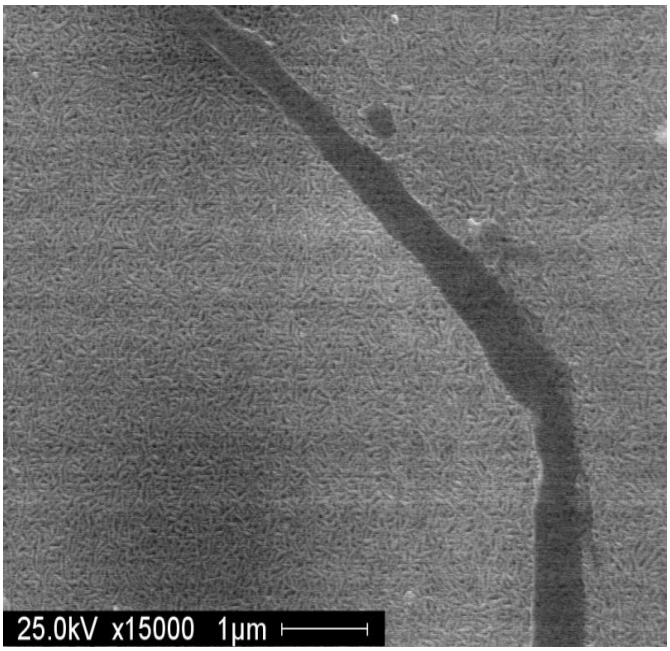

Figure 34 Imperfections arising due to improper sample cleaning and storage

4.7 Nuances in Chemical Bath Deposition

There are two types of growth of CdS films; they are Ion-by-ion growth and cluster-by-cluster growth. Ion-by-ion growth give rises to A-quality films and cluster-by-cluster growth give rises to B-quality films [19]. A-quality films are required for uniform deposition and homogenous nucleation. The speed of the magnetic stirrer is vital to the outcome of deposition. An increase in the stirring speed causes the arrival rate of Cd^{+2} and S^{-2} ions to increase. This results in precipitation of the colloidal CdS particles which grow only by ion-by-ion growth [19]. Vigorous stirring is also proven to reduce the powdery nature, physical coherence and spectacular reflectance of the films [19]. The increase in the deposition rate lowers the saturation thickness [19]. In general, the light absorbed in the CdS layer decreases the quantum efficiency in the blue part of the spectrum [20]. Thus, a less thick film, gives better quantum efficiency through the spectrum. Initially due to our low spinning speed, we formed a cluster-by-cluster growth of CdS. The precipitation on the sample was powdery and when sonication was done, the precipitated

powder fell and gave rise to pin holes. When the spinning speed was adjusted, the CdS deposition on the sample was homogenous and there were no powdery precipitates.

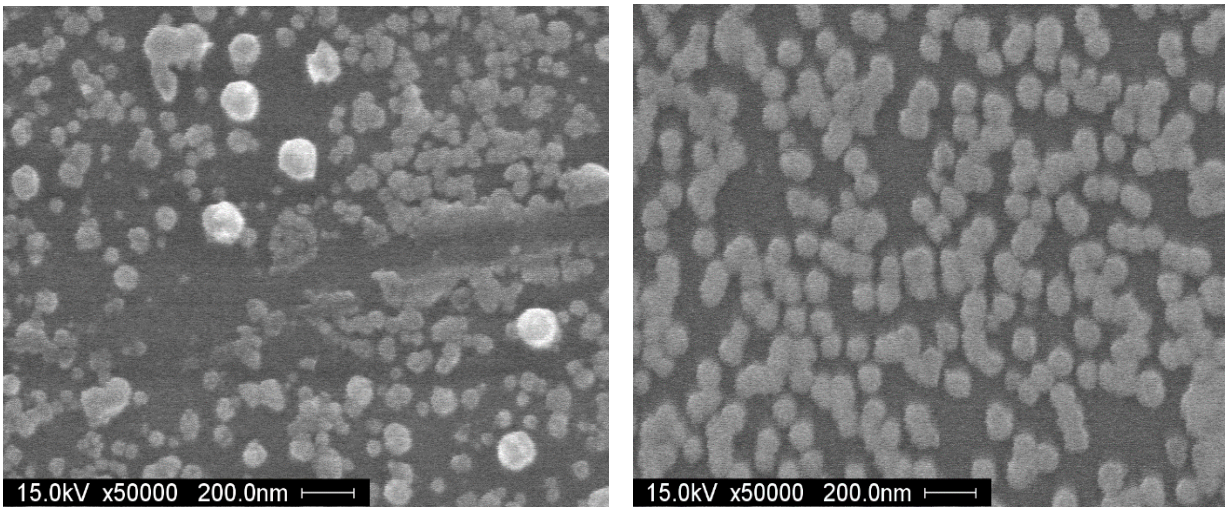

a) **b)**

Figure 35 a) Uneven grains due to low spinner speed b) Even grain growth for an increased spinner speed

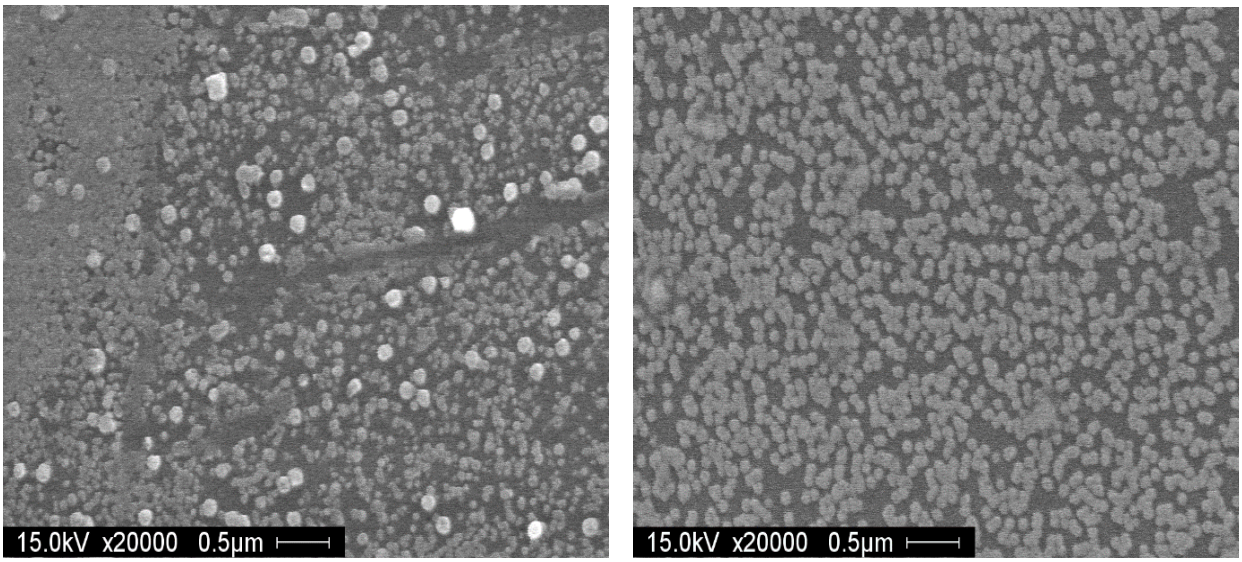

a) **b)**

Figure 36 a) Non uniform deposition due to cluster-by-cluster growth b) Uniform deposition due to Ion-by-ion growth

4.8 EDS Depth Penetration

EDS was extensively used for determining the atomic composition of elements in the CIGS solar cells. The beam voltage determines the penetration depth. For the atomic elements present in a sample, EDS beam voltage can be between ten times the lowest peak of interest and two times the highest peak of interest for accurate results. The input beam voltage for CIGS was varied for two input voltages 25KeV and 15KeV. The variation in elemental composition as function of depth is studied. A casino simulation of how far the input beam travels through the sample is also shown. The blue colored lines are the primary electron beam which creates the X-rays required for EDS analysis and the red colored lines are the backscattered electrons.

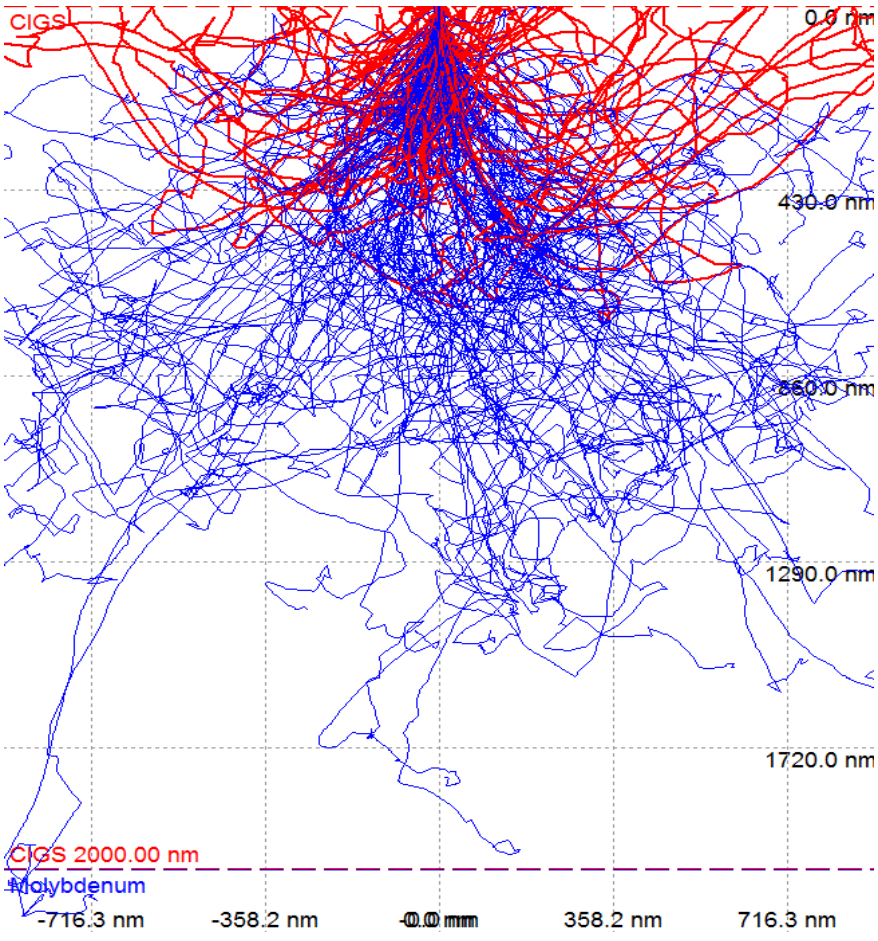

Figure 37 A depth profile simulation at 25KeV

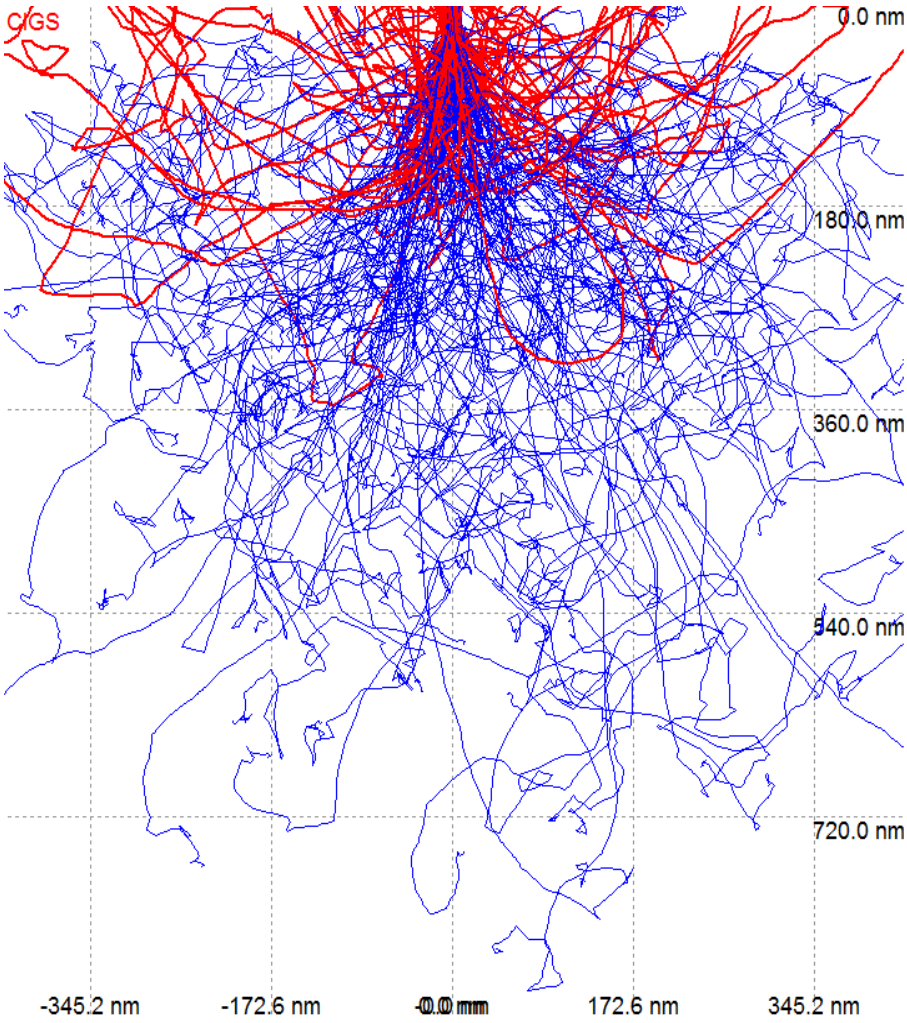

Figure 38 A depth profile simulation at 15KeV

Parameters such as the elements in the sample, thickness of the sample and the beam voltage are inputted for the simulation of depth profiling. The simulation in figure 37 shows that the obtained atomic composition for 25KeV input voltage is roughly from the first 1700 nm of the CIGS sample. The total CIGS thickness is 2000 nm (or 2 μm). Similarly, figure 38 shows that the obtained atomic information for a 15KeV input voltage is from the first 720 nm of a 2000 nm thick CIGS sample. The input voltage of 25KeV gives the in-depth detail of the sample, whereas the input voltage of 15KeV is more towards the surface. Thus grading of elemental composition with respect to the depth can be seen. Figure 39 shows the atomic composition of elements for an

input voltage of 25KeV. From the simulations above, we can roughly determine the depth of the information to be from the first 1700 nm of the 2000nm thick CIGS sample.

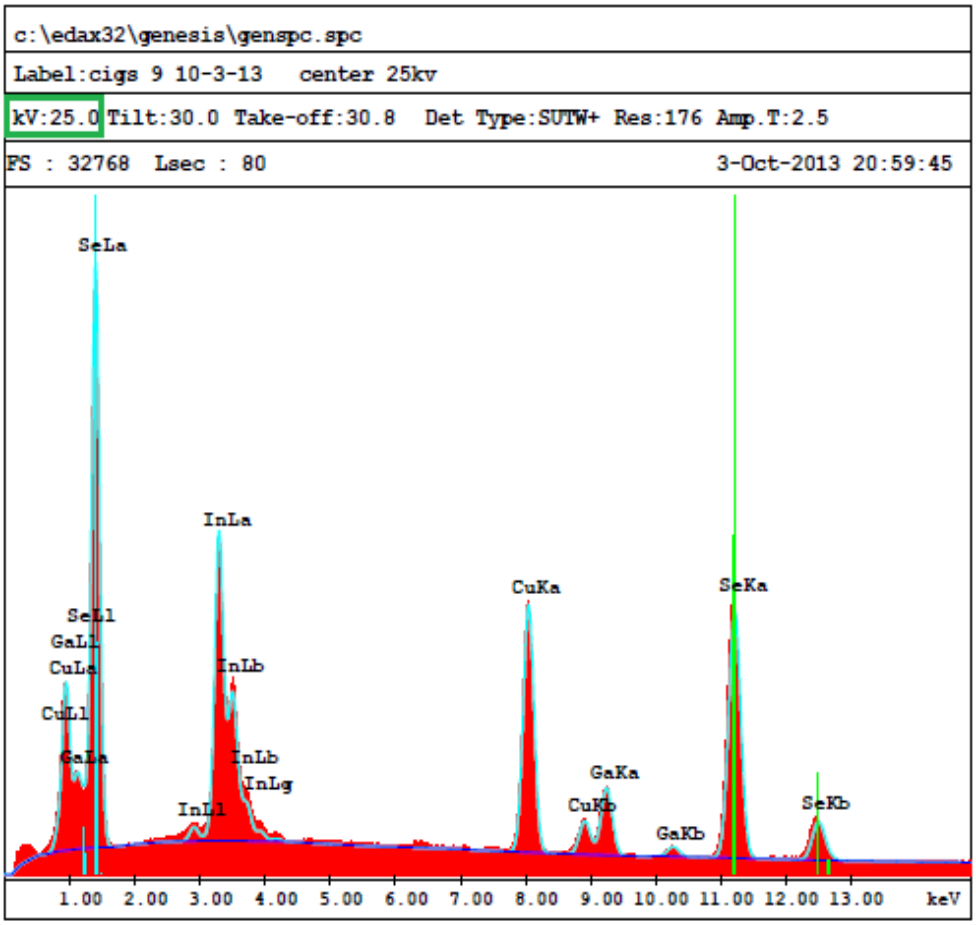

EDAX EAF Quantification (Standardless)
Element Normalized
SEC Table : Default

Element	Wt %	At %	K-Ratio	Z	A	F
InL	20.71	14.44	0.1625	0.9627	0.8153	1.0000
CuK	17.18	21.65	0.1889	1.0614	0.9656	1.0727
GaK	6.92	7.95	0.0752	1.0305	0.9583	1.1003
SeK	55.19	55.96	0.5337	0.9919	0.9750	1.0000
Total	100.00	100.00				

Element	Net Inte.	Bkgd Inte.	Inte. Error	P/B
InL	2419.84	320.74	0.25	7.54
CuK	2351.29	263.03	0.25	8.94
GaK	670.39	240.42	0.56	2.79
SeK	2662.15	224.46	0.23	11.86

Figure 39 EDS analysis on CIGS sample at 25KeV

Figure 40 shows the atomic composition of elements for the same CIGS sample at 15 KeV. This information is obtained from the first 700nm of the CIGS sample. A decline in In, Cu and Ga atomic percentages and an increase in the Se atomic percentage can be seen.

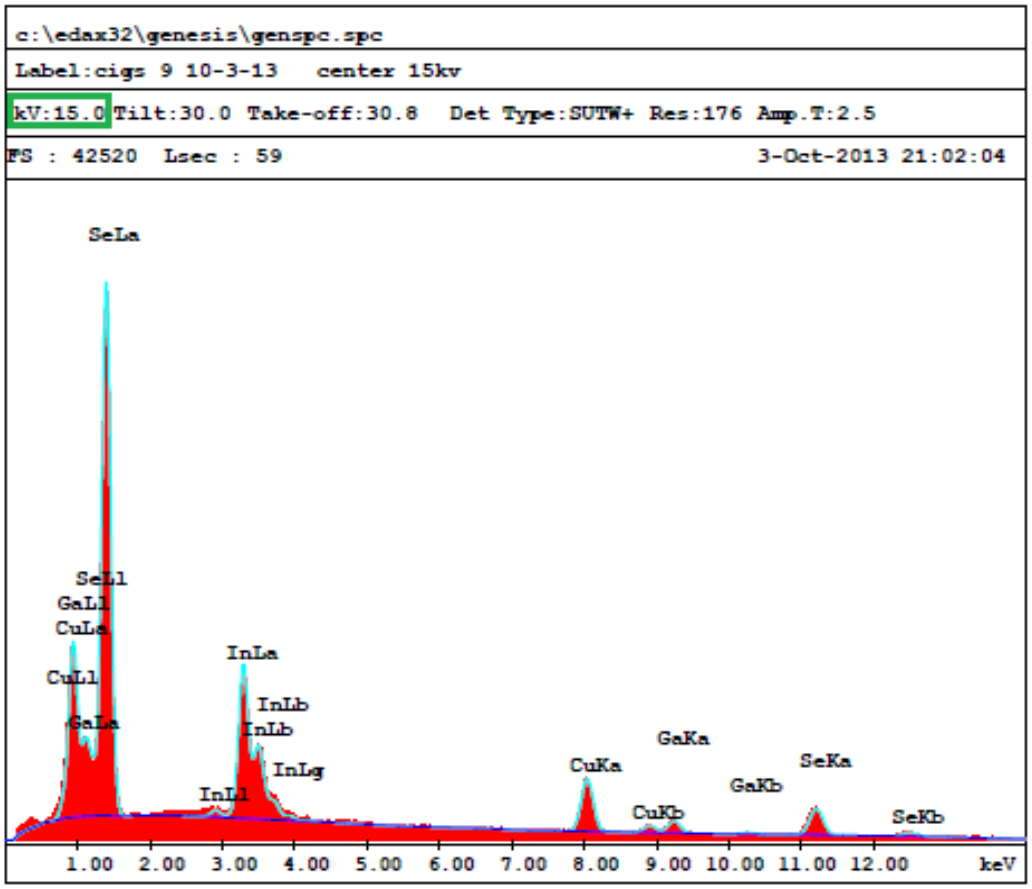

EDAX ZAF Quantification (Standardless)
Element Normalized
SEC Table : Default

Element	Wt %	At %	K-Ratio	Z	A	F
InL	12.17	8.39	0.1052	0.9577	0.9025	1.0000
CuK	11.67	14.54	0.1289	1.0771	0.9908	1.0346
GaK	5.54	6.29	0.0606	1.0419	0.9912	1.0591
SeK	70.62	70.79	0.7008	0.9957	0.9967	1.0000
Total	100.00	100.00				

Element	Net Inte.	Bkgd Inte.	Inte. Error	P/B
InL	2190.78	379.59	0.32	5.77
CuK	916.52	189.64	0.51	4.83
GaK	219.07	162.21	1.37	1.35
SeK	513.51	132.75	0.70	3.87

Figure 40 EDS analysis on a CIGS sample at 15KeV

A decline in the Ga atomic percentage from the top of the sample to the bottom confirms gallium tendency to accumulate towards the back of the device. The importance of this is already discussed in section 1.5.1.

4.9 I-V Characteristics of the Device

I-V characteristics were obtained for devices made with process 1. A Cu/III ratio of 0.78 and Ga/III ratio of 0.34 yield the following I-V characteristics.

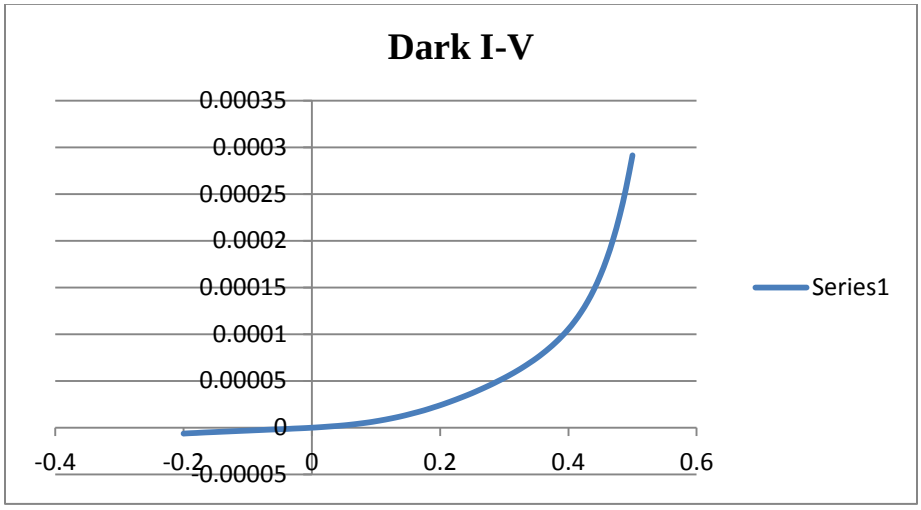

Figure 41 Dark I-V for SC-53

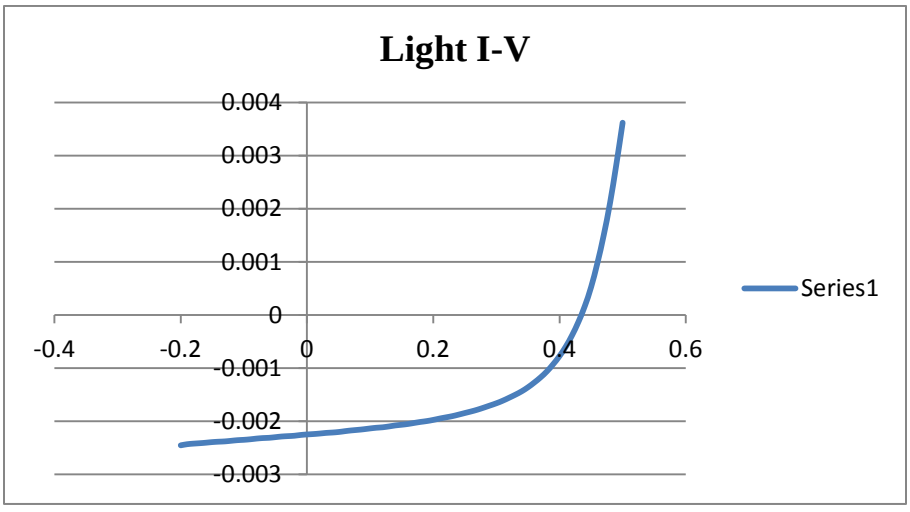

Figure 42 Light I-V for SC-53

A highest V_{oc} of 520 mV was obtained for Cu/III of 0.666 and Ga/III of 0.43. Figure 42 and 43 show the dark and light I-V curves for SC-56.

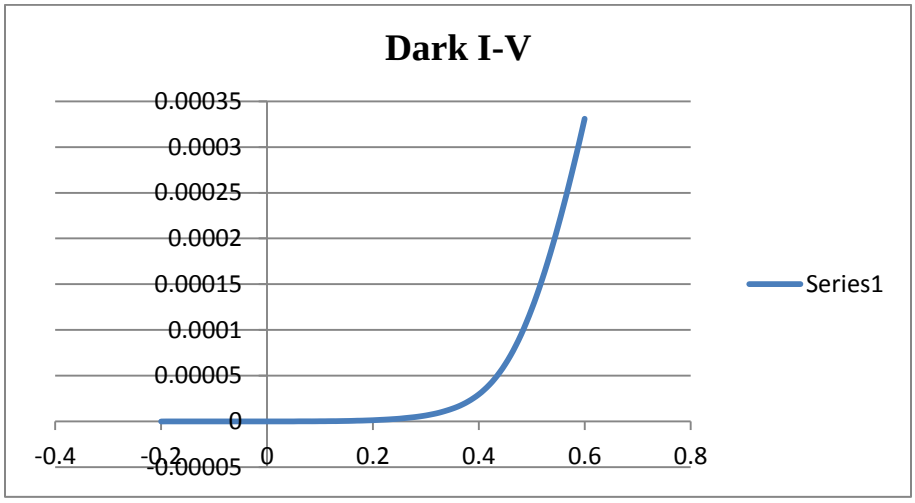

Figure 43 Dark I-V for SC-56

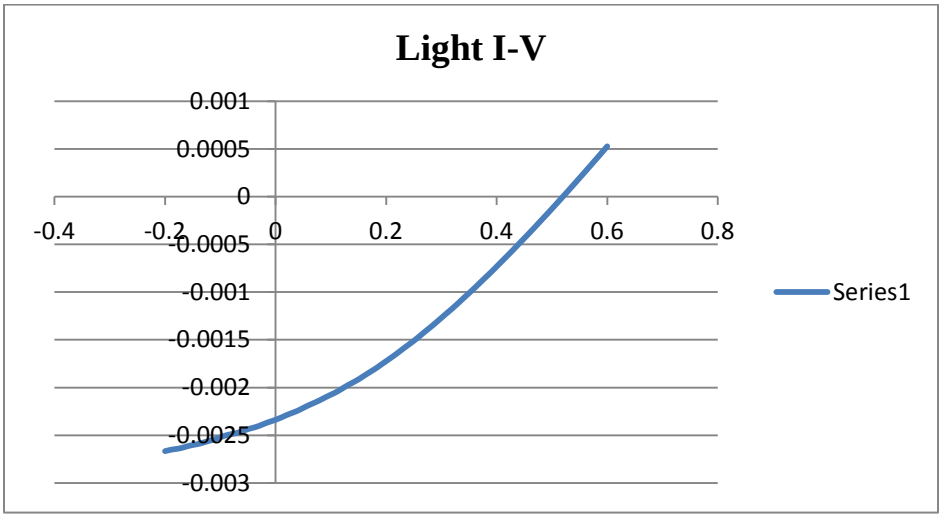

Figure 44 Light I-V for SC-56

The increase in V_{oc} is attributed to the increase in Ga/III ratio. An increase in Ga/III ratio increases the bandgap of the device thereby increasing the V_{oc}. Even though there is an increase in V_{oc} , the current and fill factors take a hit and reduce the device efficiency. This highlights the

need for the right stoichiometric balance to get optimum device performance. The best efficiency curves were obtained for Cu/III of 0.98 and a Ga/III of 0.35. Figure 44 and 45 show the dark and light I-V characteristics for SC-47.

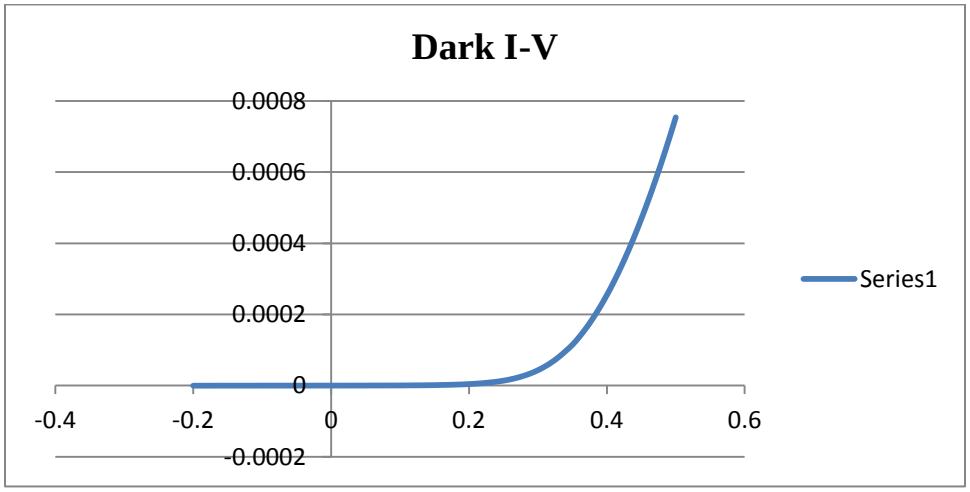

Figure 45 Dark I-V for SC-47

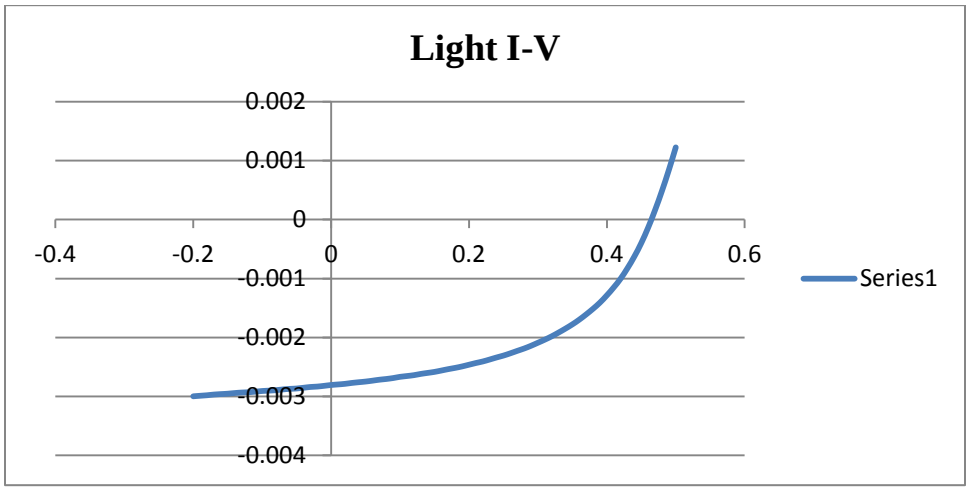

Figure 46 Light I-V for SC-47

The results of the dark and light I-V measurements for SC-53, SC-56 and SC-47 were a combined effort of my lab mate Ryan Anders and me. Ryan Anders was the lead engineer for SC-47, SC-53 and SC-56. SC-56 produced a highest cell efficiency of 6.33 %.

There was a hiatus in the solar cell manufacturing and we concentrated on developing the absorber with optimized elemental usage. When the manufacturing of solar cells resumed, we were having issues with producing solar cells with good current and fill factors. A part of this can be blamed on the top contact. The depletion of the target had reduced the conductivities of the top contact. Figure 46 and 47 shows the I-V characteristics of process 2.

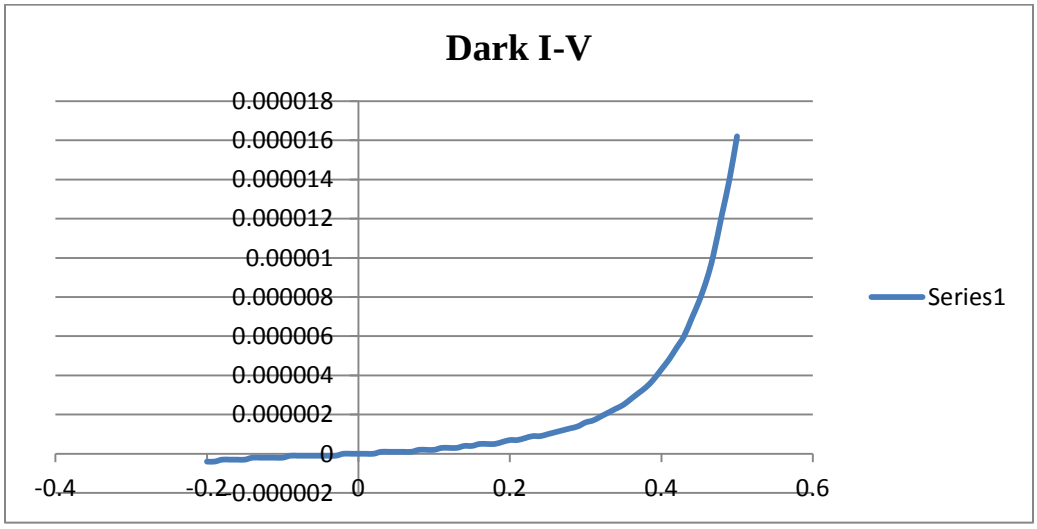

Figure 47 Dark I-V for MSC-11

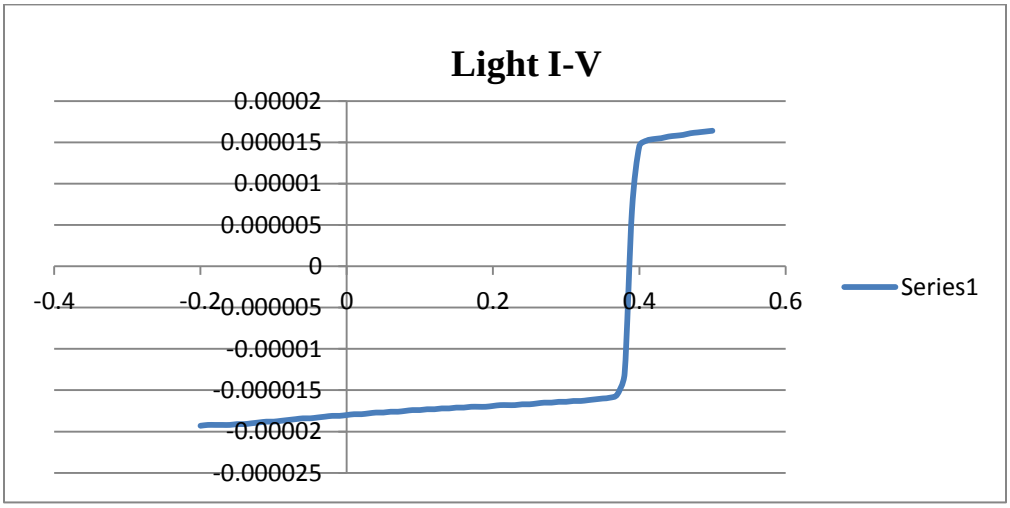

Figure 48 Light I-V for MSC-11

CHAPTER 5: CONCLUSIONS AND RECOMMENDATIONS

The objective of this thesis was to control processing the of two stage CIGS solar cells. The control of the process minimizes error and enhances throughput during commercial manufacture. Different processes have been tried to get the right recipe useful for scaling up of the process. The solar cells made with process 2 have an optimum elemental usage with the right stoichiometric balance. To achieve reproducible results with this process, it is important to follow certain guidelines. The basics of the guidelines start with the storing and cleaning process. The samples should never be stored in polymers, even prior to the cleaning process. The effect of improper sample storage can be seen on the back contact and also on the absorber. It is important to use only DI water throughout the cleaning procedure, even while soap scribing the glass samples. A proper monitoring of the Se flux is required for reproducible absorber layer. It is also helpful to understand how the evaporation rate of Se changes with temperature. It is better to do a rate monitoring test for all the effusion cells from time to time. This is because metals and metal-selenium compounds might get deposited under the thermocouples, leading to a secondary thermocouple under the effusion cell. Removing the effusion cells outside the chamber is not recommended on a regular basis. This often leads to changes in the orientation of the effusion cells which throws off stoichiometry of the absorber. Care should be taken after the deposition of CIGS absorber layer, an EDS measurement done after absorber layer deposition might be harmful for the absorber layer. EDS is always preferred to be done after CdS deposition. CdS should be done immediately after the sample is taken out of the vacuum chamber and it is preferable for the CIGS sample to remain in vacuum before the CdS deposition. Nuances in

chemical bath deposition of CdS are to be kept in mind while doing the run, mainly with the spinning rate which determines if the solution is grown by ion-by-ion growth or cluster-by-cluster growth. The quantitative readings from the EDS after CdS deposition cannot be taken as such. We must understand that there is a slight error involved and should be open to the idea of a plus or minus 5-10% error. Also the quantitative amount of Cd and S in the overall EDS data, throws the ratio of CIGS a bit. Another factor to be wary of during the processing of CIGS solar cells is the top contact. The top contact, ZnO:Al, is very sensitive to oxygen present inside the vacuum chamber. A low base pressure (< 6 μT) is to be maintained prior to the deposition. Heating the chamber before achieving the base pressure also helps in reducing the partial pressure of oxygen inside the chamber by releasing all the water vapor molecules sticking to the chamber walls. It is important to have a temperature of at least 125℃ during the ZnO:Al top contact deposition. Thus a propitious process for two stage CIGS solar cells was developed. A better control during the growth process and a reproducible device stoichiometry was achieved. The process has great potential to enhance throughput of commercial manufacture of CIGS solar cells. Further improvements in the process can be made with better conductivity of the top contact.

REFERENCES

[1] Jenny Nelson, Book: *The physics of solar cells*, Imperial college press, (2003).

[2] Experience,Inc. (2013), *Experience,Inc publishes an article on The History Of Solar Power*, Retrieved August 15, 2013 from http://www.experience.com/alumnus/article?channel_id=energy_utilities&source_page=additional_articles&article_id=article_1130427780670

[3] The Economist, *The Economist publishes an article on The Rise Of Solar energy*, Retrieved August 15, 2013 from http://www.economist.com/blogs/graphicdetail/2012/12/daily-chart-19

[4] The Economist, *The Economist publishes an article on Alternative Energy Will No Longer Be Alternative*, Retrieved August 15, 2013 from http://www.economist.com/news/21566414-alternative-energy-will-no-longer-be-alternative-sunny-uplands

[5] Martin A. Green, Ryne P. Raffaelle, Tim M. Bruton, Book: *Progress in Photovoltaics: Research and Applications*, ISI Journal Citation Reports, (2009).

[6] Hans J Moller, Book: *Semicondutctors for Solar Cells*, Artech House, (1993).

[7] Zhang Xuan, Rajendiran Aravind Raj, Wu Yiming,"*Analyzing Hi-Technology opportunities CIGS solar cells*", (2011).

[8] Jef poortmans, Vladimir Arkhipov, Book: *Thin film Solar cells: Fabrication, characterization and application*s, John Wiley and Sons, Ltd

[9] Andrew M. Gabor,"*The conversion of* $(In,Ga)_2Se_3$ *thin films to* $Cu(In,Ga)Se_2$ *for application to photovoltaic solar cells*", Doctoral dissertation, University of Colorado, (1995).

[10] Albin, D.S., et al., *Materials Research Society Symposium Proceedings.* 228, p. 267 (1991).

[11] Dominik Rudmann, "*Effects of sodium on growth and properties of Cu(In,Ga)Se_2 thin films and solar cells", Doctoral dissertation, Swiss Federal Institute of Technology*, (2004).

[12] Elif Selin Mungan, Xufeng Wangand and Muhammad Ashraful Alam, "*Modeling the Effects of Na Incorporation on CIGS Solar Cells*", IEEE journal of photovoltaics, Vol.3, No.1.

[13] S.H. Wei and A. Zunger, "*Band Offsets and Optical Bowing of Chaclcopyrites and Zinc-Based II-VI Alloys*", Journal of Applied Physics, 78, 6, 3846, (1995).

[14] L. Weinhardt, C. Heske, E. Umbach, T. P. Niesen, S. Visbeck et al., *Band alignment at the i-ZnO/CdS interface in Cu(In,Ga)(S,Se)2 thin-film solar cells*, Appl. Phys. Lett. 84, 3175, (2004).

[15] Shirish A. Pethe, Eigo Takahashi, Ashwani Kaul, Neelkanth G. Dhere,"*Effect of sputtering process parameters on film properties of molybdenum back contact*", Solar energy materials and solar cells, Volume 100, page 1-5, (2012).

[16] Jun Young Choi, Kang-Jin Kim, Ji-Beom Yoo and Donghwan Kim,"*Properties of cadmium sulfide thin films deposited by chemical bath deposition with ultrasonication*", Solar Energy Vol. 64, Nos 1–3, p. 41–47, (1998).

[17] M.Contreras, B. Egaas, K. Ramanathan, J. Hiltner, F. Hasoon, R. Noufi, *Prog. Photovoltaics*, 7, 311, (1999).

[18] B. Marsen., S. Marsillac., S.Dom, R.Rocheleau,"*Effect of selenium effusion rate on CIGS thin films deposited at low substrate temperature*", Photovoltaic Specialists Conference, Conference record of thirty-first IEEE, p. 386 – 389, (2005).

[19] Inderjeet Kaur, D. K. Pandya, and K. L, Chopra,"*Growth Kinetics and Polymorphism of Chemically Deposited CdS Films*", Department of Physics, Indian Institute of Technology, Delhi, New Delhi 110029, India.

[20] H.R. Moutinho, R.G. Dhere, M.M. Al-Jassim, C. Ballif, D.H. Levi, A.B. Swartzlander, M.R. Young, L.L. Kazmerski," *Proceedings of the 28th IEEE Photovoltaic Specialists Conference, Anchorage*", U.S.A., September 15-22, p. 646, (2000).

[21] Keshavanand Jayadevan, "*Fabrication and Characterization of Novel 2SSS CIGS Thin Film Solar Cells for Large-Scale Manufacturing*", University of South Florida, (2011).

[22] K. Jayadevan, R. Anders, S. Zafar, C.S. Ferekides, D.L. Morel, " *Selenization pathways for 2SSS CIGS manufacturing*", 37th IEEE PVSC, (2010).

[23] A. Rockett et al, "*Structure and chemistry of $CuInSe_2$ for solar cell technology: Current understanding and recommendations*", Thin Solid Films, 237, (1994).